Photocopy and Use Authorization

In presenting this thesis in partial fulfillment of the requirements for an advanced degree at Idaho State University, I agree that the Library shall make it freely available for inspection. I further state that permission for extensive copying of my thesis for scholarly purposes may be granted by the Dean of Graduate Studies, Dean of my academic division, or by the University Librarian. It is understood that any copying or publication of this thesis for financial gain shall not be allowed without my written permission.

Signature: ____________________________

Date: ________________________________

Water-driven Basalt Alteration: Kilauea, Hawai'i as an Analog for Mars

by

Stacy Henderson

A thesis

submitted in partial fulfillment

of the requirements for the degree of

Master of Science in the Department of Geosciences

Idaho State University

Summer 2020

Committee Approval

To the Graduate Faculty:

The members of the committee appointed to examine the thesis of STACY HENDERSON find it satisfactory and recommend that it be accepted.

Dr. Shannon Kobs Nawotniak,
Major Advisor

Dr. Michael McCurry,
Committee Member

Dr. Andrew Holland,
Graduate Faculty Representative

Acknowledgements

First and foremost, I would like to thank Dr. Shannon Kobs Nawotniak for the opportunity to participate in this research. She was an amazing advisor and mentor who believed in me and helped me to believe in myself. I'd also like to thank the Idaho State University Geosciences Department faculty and staff for all of their support and guidance, both academically and personally.

I'd like to thank Dr. Darlene Lim and NASA for the NASA Planetary Science and Technology Through Analog Research (PSTAR) program (NNH14ZDA001N-PSTAR) grant to Dr. Darlene Lim.

A huge thank you to Dr. Michael McCurry (former department chair and my committee member) for all his help and guidance. I learned so much from him, the passion after so many years of doing this work is still evident and contagious. Thank you to Dr. Andrew Holland, my GFR, for being willing to answer the multitude of chemistry questions I had. I learned so much in a short amount of time.

I would also like to thank Kyla Grasso for the empathetic ear, amazing hugs, mountain bike rides, trail runs, x-country ski days (and nights), coffee dates, social distancing dates at the park, which were much needed breaks from the grind of graduate school life. Emma Greggory and Matt Wierenga, thanks for wine, beers, study sessions and everything else. Tyler Paladino and Sara Warix for always inviting me climbing and mountain biking. And all the grad students both past and present that were always up for fun. You all made my time at ISU one of the most amazing and memorable experiences of my life. Thank you all!

Table of Contents

List of Figures

List of Tables

Water-driven Basalt Alteration: Kilauea, Hawai'i as an analog for Mars

Thesis Abstract – Idaho State University (2020)

This project examines water-altered basalts from Kilauea as an analog to Mars to understand alteration products and degrees of change associated with various styles of water-rock interaction; the value of this work is to better understand potential microbial habitability of past systems on Mars. We compare altered basalts from Mauna Ulu, Kilauea Iki, and the Kilauea Caldera floor to unaltered rocks from within the same flows using XRF, petrography, and SEM/EDS. In the magmatic fumaroles, rocks were strongly enriched in TiO_2, SiO_2, and S. The meteoric fumarole systems exhibited minor enrichment in SiO_2, MgO and Fe_2O_3. Rocks from magmatic systems are more thoroughly altered than those in meteoric systems due to the increased temperature and acidity of the associated water. Preliminary comparisons with microbial and organic geochemistry results indicate that true analog comparisons may only be possible through the most extreme fumarolic conditions, as microbial colonies at the lower-alteration Mauna Ulu sites are dominated by non-endolithic extremophiles.

Keywords: Mars, fumarole, basalt, Kilauea, Hawaii, alteration, analog, microbial

Chapter 1: Introduction

1.1 Purpose

Mars is within the habitable zone of the sun, making it a key target in NASA's search for life outside of our planet. While Mars is currently dry and cold, it may have been relatively warm and wet during the Noachian and Hesperian periods (4.1 – 2.9 billion years (Ga)) and had active volcanism (Pollack et al., 1987; Craddock and Howard, 2002; Vago et al., 2017). These conditions could have created habitats suitable for microbial communities that live within rocks, and would have utilized hydrothermally altered basalt for energy and nutrients (Dunfield and King, 2004; Costello et al., 2009; Callac et al., 2013; Cockell et al., 2013, 2019). While endolithic microbial communities have been hypothesized for Mars, we currently do not know which water-rock alteration states would have offered the best chances for habitability, and, therefore, do not know which rocks to target for closer investigation in search of evidence of past life.

It has been hypothesized that life on Earth began in hydrothermal systems associated with basaltic volcanism (Horneck, 2000; Konhauser et al., 2002; Walton, 2008; Djokic et al., 2017; Damer and Deamer, 2020). Water-rock interaction has the potential to change the mineralogical state of elements within the rock as well as the bulk chemistry. This is important to the search for extraterrestrial life, which may occur as endolithic microbes, as these changes potentially make the rock more or less habitable (Horneck, 2000; Al-Hanbali et al., 2001; Varnes et al., 2003). Understanding the mineralogical and geochemical changes that are caused by different warm water and basalt reactions as well as the spatial scales over which these changes occur are important steps toward identifying the best locations to search for past life on Mars. I hypothesize that water type (e.g. magmatic vs. meteoric) has the largest influence on the extent of alteration a rock undergoes and magmatic fumaroles will exhibit the greatest degree of alteration.

This work expands on past efforts by Naughton et al. (1976), Barnard et al. (1990), and Hurwitz et al. (2003), which focused on the geochemistry of magmatic fumaroles; research of meteoric water-basalt interaction (Gislason and Eugster, 1987; Gislason et al., 1993); and chemical weathering of basalt (Eggleton et al., 1987; Li et al., 2016). In order to further explore which environments on Mars may be most suitable for life, we examined the mineralogy and geochemistry of five different hydrothermal systems encompassing three alteration styles on Kilauea Volcano, Hawai'i. We investigated active and relict magmatic fumaroles on the Kilauea caldera floor, relict meteoric fumaroles on Kilauea Iki, and active and relict meteoric fumaroles and syn-emplacement alteration on Mauna Ulu. We also sampled unaltered rock from each flow to provide a baseline for determining the extent of any changes brought on by water-rock alteration at each location. We also examined smaller spatial gradients within fumarolic systems to understand how conditions changed from the center of the vent to its margin (1-2 m halo from center of the vent). The composition profiles assembled by this study will be used in combination with microbiology and organic geochemistry studies by our partners on the BASALT project to better predict which water-rock interactions are most likely to have supported microbial life on Mars. The results of this work may be used in the future to guide our robotic and/or manned missions to Mars to search for life on the red planet.

1.2 NASA

This research was carried out as part of the NASA BASALT (Biologic Analog Science Associated with Lava Terrains) research project. We are entering a new age of space exploration, with the return of crewed missions to the Moon for the Artemis Program beginning in 2024 and goals to send humans to Mars after that. This return to space exploration is driven by scientific questions, including: Is there evidence of past microbial life on Mars? The NASA BASALT project was created to address this question while simultaneously investigating how to carry out science-driven missions operating across significant time delays between the field team and mission control. BASALT used an interdisciplinary approach to investigate endolithic microbial inhabitation associated with water-rock interaction in Mars-analog environments on Earth, with field areas at Craters of the Moon National Monument and Preserve, ID, and Hawai'i Volcanoes National Park, HI (e.g., Brady et al., 2019; Cockell et al., 2019; Hughes et al., 2019; Kobs Nawotniak et al., 2019; Lim et al., 2019).

This thesis encompasses the Hawaiian geology portion of the BASALT project, which sought to understand variations between different modes of water-rock alteration including mineral and chemical changes and the relevant scales over which these changes occur. These results can be combined with microbiology and organic geochemistry findings to understand how habitability of endolithic microbial communities change in different environments and along different spatial gradients. By conducting the BASALT study as a multidisciplinary approach, each team is able to analyze the same suite of rock samples representing various spatiotemporal characteristics, thereby enabling strong correlation potential between the various sets of analytical results. Through this approach, we get a good snapshot of alteration styles, habitability, community types, and biomass amounts at one specific moment in space and time. This thesis reports on geologic research carried out on Kilauea Volcano during the 2016 and 2017 field deployments, which I did not participate in. While this thesis includes some discussion of microbiology and organic geochemistry results in relation to the mineralogy and inorganic geochemistry for the Mauna Ulu sample suites, there are not yet biologic results for the Kilauea Iki or Kilauea caldera floor suites.

Sample collection methods for this project differ from traditional field methods. Field work for the BASALT deployment was conducted as a simulated crewed Mars mission consisting of multiple teams. The teams for the simulation consisted of astronauts in the field (EV) and in a "Mars habitat" (IV), a team of interdisciplinary experts in a Science Backroom Team (SBT) in the Mission Support Center, and engineers who ensured that the Mars- and Earth-based parts of the team communicated using tools and time delays consistent with anticipated future missions to Mars (e.g., Lim et al., 2019). The field astronauts were outfitted with earpieces, microphones, video cameras, wrist-mounted digital maps, continuous-tracking GPS, DSLR cameras, scale bars, sterilized rock hammers, sterile Whirl-Pak sample bags, multiple handheld spectrometers, and other needs for the day (Lim et al., 2019). Most of the equipment carried by EV astronauts was used for communication and context with both the IV team and the SBT on Earth (Beaton et al., 2019a)

Communications between SBT and astronauts on Mars were conducted mainly via text messaging to the IV team, who then communicated via voice with the EV team (Beaton et al., 2019b; Kobs Nawotniak et al., 2019). This method allowed for clearer communication between teams: the text format mitigated confusion and interruptions over the 5- and 15-minute latency communication between SBT and IV, and the voice communication between EV and IV was part of a continuous conversational flow that supported hands-free communication in the field (Kobs Nawotniak et al., 2019). The text method also allowed for the Earth based SBT to send maps that could be used to guide the EV team (Beaton et al., 2019b). The EV team wore chest mounted cameras that sent constant video to IV and then SBT; still images were also sent to SBT to help with context and sample selection (Kobs Nawotniak et al., 2019). The team used a cycle-based workflow in which EV first surveyed target zones for outcrops with the potential to meet the day's sample objectives, then returned to use hand held spectrometers on the proposed locations that SBT preferred, and finally completed actual suite sampling (Beaton et al., 2019b). By organizing the efforts by activity, rather than the more traditional field approach of completing the work at an outcrop before moving on, the SBT was given time to receive and review field photos and instrument data, reach a consensus on preferred locations for further investigation, and reply to the EV/IV teams through communication latency without having to pause the simulation (Beaton et al., 2019b, 2019a, Stevens et al., 2019) Sample collection was carried out under sterile conditions, including sterilized rock hammers, gloves, and sample bags; microbiology and organic geochemistry samples were transferred to freezer storage as soon as they were returned from the field (Cockell et al., 2019; Brady et al., *in review*).

The objectives for each field day were determined *a priori* and provided to all team members during daily morning briefings (Payler et al., 2019). The team desired samples of unaltered rock from each study area to be used as a baseline from which to measure alteration. In addition, sample targets included syn-emplacement alteration from volatile exsolution, active and relict meteoric fumaroles, and active and relict magmatic fumaroles, depending on availability in the different field zones and evolution of the guiding questions between subsequent field deployments (Hughes et al., 2019). For the active fumaroles, the SBT requested samples taken from the center or margins of the feature (2016) or from specific *in situ* temperature ranges (2017), depending on the that year's mission objectives. A full sample suite for a specific location included one piece of rock ~10 cm across and rock chips for geology, two pieces ~15 cm across for organic geochemistry, three pieces 3-5 cm across for microbiology, one piece >20 cm across for porosity/permeability, and one piece ~10 cm across for archival reference; all samples within a suite were expected to be materially the same as one another and collected from within as small an area as possible (Brady et al., 2019; Stevens et al., 2019).

Though beneficial for planning future crewed missions to Mars, the simulation nature of the BASALT fieldwork resulted in fewer samples being collected than could have been collected during the course of standard fieldwork. The Science Operations aspects of BASALT have, however, helped us understand how future manned missions to the moon and/or Mars can be accomplished in order to achieve the goal of science-oriented missions. The most profound finding the Science Operations of the BASALT program has been that it is actually possible to enable intra-EVA Earth-based science support of crewed missions (Beaton et al., 2019b). Further, the success of intra-EVA scientific support was not limited to conditions with 5-minute (low) latency or high bandwidth that allowed video streaming from the field; the SBT reported that they were fully capable of operating successfully under 15-minute latency and low-bandwidth (no video) conditions. In all of the study conditions, the systematic feed of information between SBT on Earth and EV/IV teams on "Mars" allowed consistent tracking of updated science priorities and resulted in no idle time during the EVA (Beaton et al., 2019b).

1.3 Organization

This thesis is broken down into introduction (1) and background (2) chapters followed by a manuscript chapter (3). The third chapter is written as a full manuscript to be submitted to the journal Planetary Space Science. The final chapter of this thesis contains a broad discussion focusing on inferences made during this research and ideas for future research (4).

Chapter 2: Background

2.1 Analog Justification

Earth analogs have long been used to understand extraterrestrial bodies and help answer questions about similarities between Earth, the Moon, and Mars (Wilson and Head, 1981, 1983), martian geology and geochemistry (Greeley and Spudis, 1981; Allen et al., 1981; Edwards et al., 2008), existence of water on Mars (Baker, 2001; Craddock and Howard, 2002), martian atmospheric conditions (Forget, 1997; Haberle, 1998), and microbial habitability (Horneck, 2000; Cockell, 2014; Davila and Schulze-Makuch, 2016). We chose Kilauea, HI for this study due to its legacy as an analog site (Greeley, 1974), similarity to the basalts of Mars (Morris et al., 2000), presence of sulfur (King and McLennan, 2010), presence of opaline silica encrustations (Chemtob and Rossman, 2014), a warm and wet environment (Ingebritsen and Scholl, 1993), and minimal contamination from continental rocks (Garcia et al., 1998).

Mars experienced extensive volcanism during the late Noachain to early Hesperian period (ca. 3.7 – 3.1 Ga), and evidence indicates that there have been eruptions < 100 Ma (Neukum and Hiller, 1981; Hauber et al., 2011). Volcanism on Mars is dominated by effusive basaltic lava flows and episodes of shield building, which are similar to the eruptions of Kilauea (Greeley and Spudis, 1981; Wilson and Head, 1983; Wolfe and Morris, 1996; Sigurdsson et al., 1999). The martian surface is predominantly composed of basalt in the southern highlands and basaltic andesite or weathered basalt in the northern lowlands (Bandfield, 2000; Wyatt and McSween, 2002). Previous Mars missions found tholeiitic basalts that are similar to those of Kilauea in the Valles Marineris and Ares Vallis regions that lie between the southern highlands and northern lowlands near the equator (Figure 1) (Morris et al., 2000; Edwards et al., 2008).

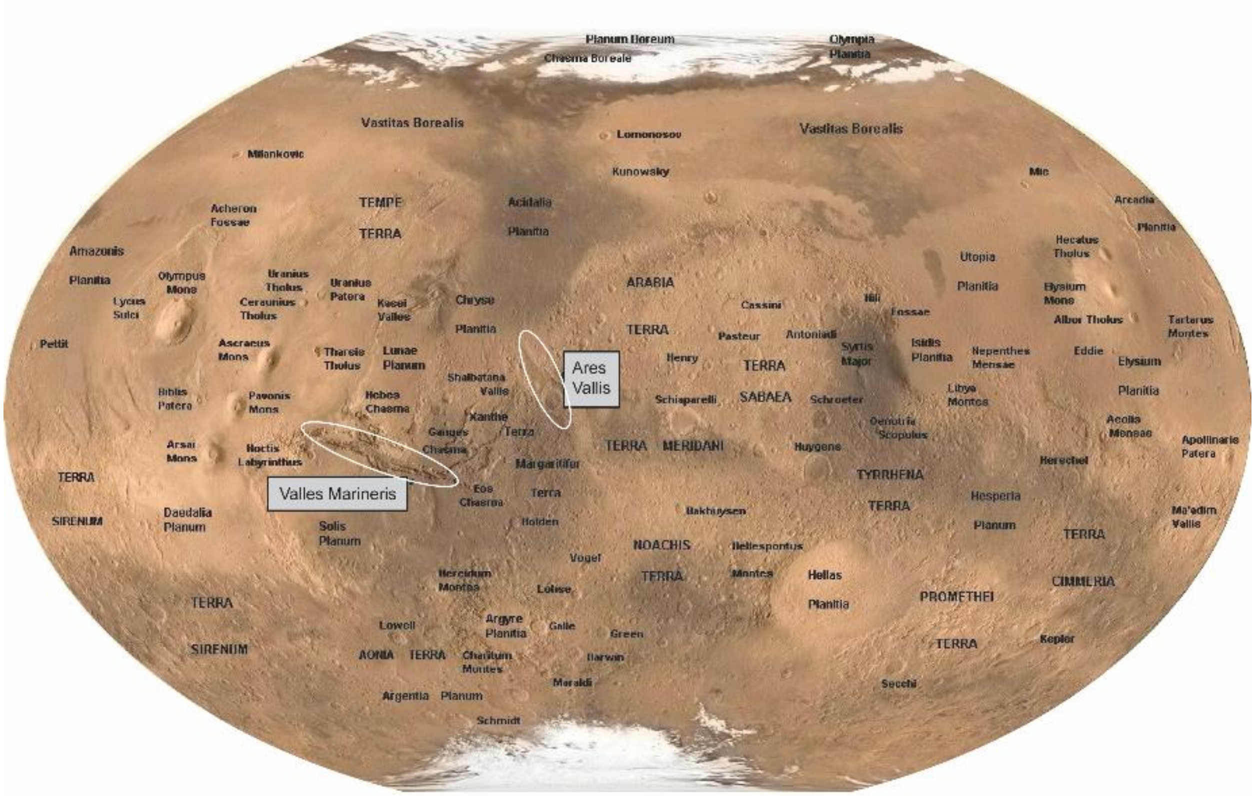

Figure 1: Map of Mars with the Ares Vallis and Valles Marineris shown in white ellipses. Image: National Geographic Society, MOLA Science Team, MSS, JPL, NASA. Caption credit: Alwyn Botha.

Evidence of surface water has been found on Mars in the form of fluvial valleys, rounded cobbles, sedimentation, hydrated minerals, and clays dating to the late Noachian to early Hesperian and as recently as 1000 – 600 Ma (Baker, 2001; Jakosky and Phillips, 2001; Grotzinger et al., 2014; Vaniman et al., 2014; Ehlmann and Edwards, 2014). The Mars rover Opportunity found high silica rocks and soils on the martian surface consistent with opaline silica, which was later verified by the Mars rover Spirit (Squyres et al., 2008; Ruff et al., 2011, 2020). The discovery of opaline silica on Mars indicates that there were once hydrothermal systems on Mars, meaning heat and water were present and could have provided microbial habitats (Squyres et al., 2008; Damer and Deamer, 2020).

Kilauea has inherent limitations as an analog site, as do all terrestrial sites used in analog studies. Although similar, the basalt compositions differ on Kilauea and Mars: the Fe-content is higher on Mars than on Kilauea, ca. 18% and 11%, respectively. Martian basalts are also depleted in TiO_2 and Al_2O_3 compared to those on Kilauea (**Error! Reference source not found.**) (Bridges and Warren, 2006; Jackson et al., 2012).

Table 1: Average weight percent of major element oxides for basalts from Mars and Kilauea (Bridges and Warren, 2006; Jackson et al., 2012).

	SiO_2	**TiO_2**	**Al_2O_3**	**Fe_2O_3**	**MnO**	**MgO**	**CaO**	**Na_2O**	**K_2O**	**P_2O_5**
Mars	42.77	0.84	6.60	17.45	0.41	12.62	9.01	1.08	0.29	0.40
Kilauea	50.24	2.38	12.69	11.29	0.17	9.97	10.44	2.15	0.43	0.24

Another limitation of the Earth analog is difference in atmospheres between the two planets. The atmosphere on Earth contains 78% N_2, 21% O_2, and trace amounts of other gases (Atmosphere, 1976). The martian atmosphere contains 95% CO_2, 2.6% N_2, and trace amounts of other gases including oxygen (0.16%) (Franz et al., 2017; Trainer et al., 2019). This distinct difference in atmospheric chemistry could have changed how the martian basalts altered as a result of hydrothermal activity, however this is currently unknown. Therefore the analog necessarily requires the assumption that hydrothermal alteration of basalt on Mars was similar to that of modern day Kilauea. While Mars is currently cold and dry, it is hypothesized to have had a warm and wet period that was shorter lived than that of Earth, and was possibly periodic rather than sustained (Baker, 2001; Craddock and Howard, 2002). In order for the CO_2 rich atmosphere of Mars to have created conditions that would allow for surface water the atmospheric pressure would have needed to be 1 – 5 bars, up to 5 times greater than the atmosphere of Earth today at ~

1 bars (Pollack et al., 1987; Haberle, 1998). Another important factor to take into consideration for Kilauea as an analog is the chance for eolian contamination of the basalt from both continental material and microbes from oceans and rainforests. In addition, there's a risk for microbial contamination from tourists that go into closed areas. While using an totally uninhabited basaltic island would have minimized some of these issues, doing so would have resulted in significantly greater logistical challenges and cost.

2.2 Geologic setting

Kilauea is located on the Big Island of Hawai'i and consists of basaltic shield volcanoes, lava flows, cinder cones, and the Halema'uma'u lava lake and caldera (Greeley and Spudis, 1981; Wilson and Head, 1983; Sigurdsson et al., 1999). The standard lifecycle of Hawaiian volcanoes consists of the submarine stage that erupts alkalic basalts, subaerial shield-building stage consisting of tholeiitic basalts that account for > 95% of the volume of basalt on the volcano, followed by erosional and alkalic eruption stages (Clague and Dalrymple, 1987). Kilauea volcanism is currently in the shield building stage and composed of young eruptions, 90% of which are <1100 years old (Holcomb, 1987). The basalts of Kilauea are tholeiitic, meaning they contain 52 – 63% SiO_2, are Fe-rich > 9.0 wt. % Fe_2O_3 (all FeO/Fe_2O_3 reported as Fe_2O_3 in this thesis), and contain Ca-plagioclase, Mg- and Ca-pyroxenes, and Mg- Fe-olivine in a fine-grained to glassy (tachylite) groundmass similar to those found on Mars (Sun et al., 1979; Sigurdsson et al., 1999).

Hydrothermal systems on Kilauea alter rocks through various processes including syn-emplacement degassing and post-emplacement magmatic and meteoric fumaroles. Fumaroles are vents or openings near volcanoes that emit steam and gases. Fumaroles can be meteoric, sourced from water local groundwater, or they can be magmatic, in which meteoric waters have been mixed with volatiles such as H_2O, CO_2, SO_2, HCl, H_2S, and HF, that have exsolved from a magmatic body (Barnard et al., 1990).

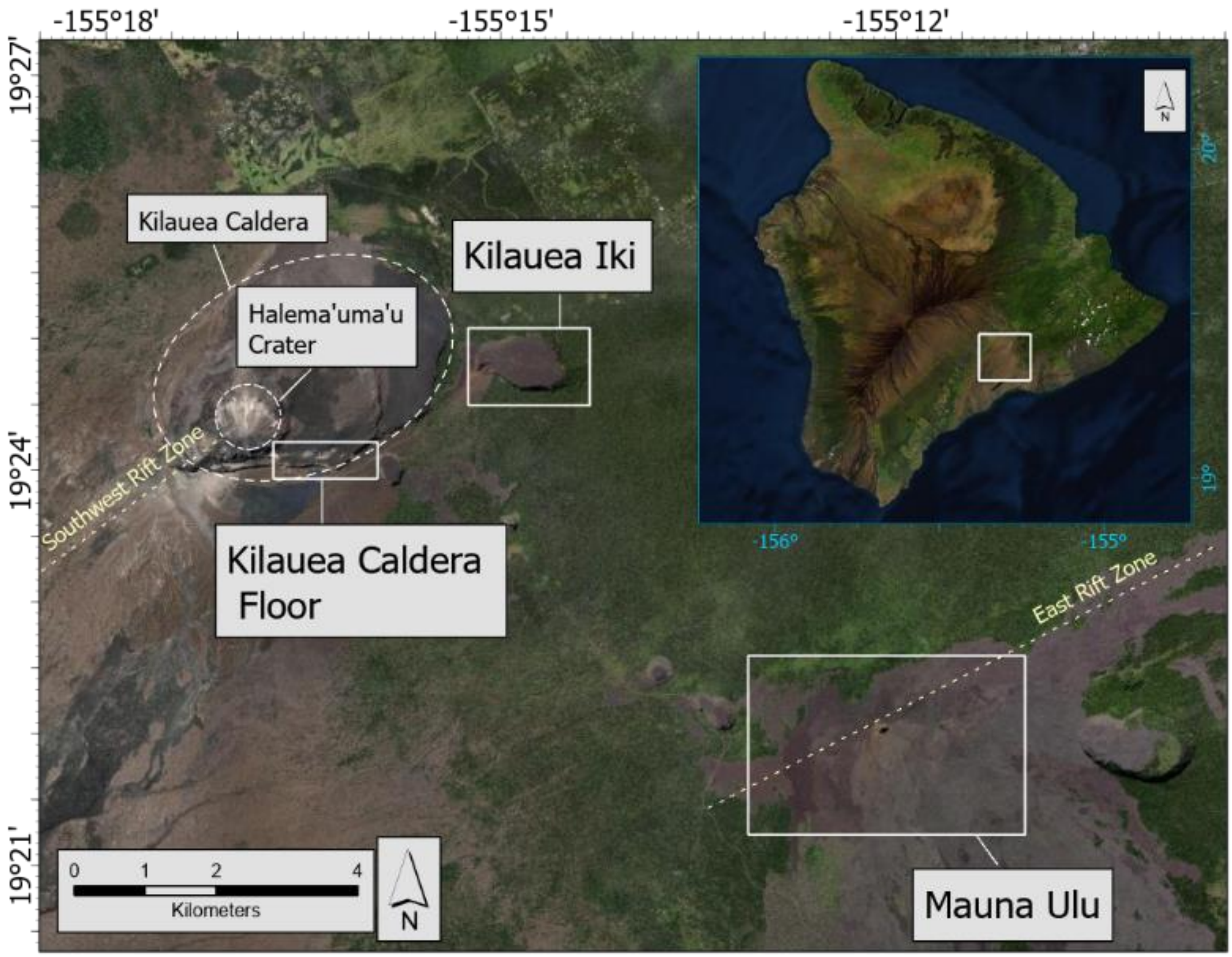

Figure 2: Location of study area showing the Big Island of Hawai'i and study area and the zoomed in map of flows sampled. Map source: Esri, Maxar, GeoEye, Earthstar Geographics, CNES/Airbus DS, USDA, USGS, AeroGRID, IGN, and the GIS User Community.

Three different basalt flows on Kilauea were studied in this project: Kilauea caldera floor near the Halema'uma'u lava lake, Kilauea Iki, northeast of the Kilauea caldera, and Maua Ulu, located south east of the Kilauea (Figure 2).

2.2.1 Kilauea Caldera Floor

The fumarolic system we sampled is located within the lavas that erupted on the Kilauea caldera floor in August 1971. The lava erupted from fissures along the southeast part of the crater as lava fountains and effusive flows (Duffield et al., 1982). This eruption is located on the summit caldera of Kilauea. A summit caldera is a large, round depression that forms at the summit of a volcano when the edifice collapses into an area where subsurface material was removed during the course of an eruption.

The Kilauea caldera floor lies above the summit magma chamber of the Kilauea volcano. Summit fumaroles near the Halema'uma'u crater are sourced from meteoric waters that contain volatiles from the magma located beneath the volcano. The mixing of meteoric water and magmatic gases here has resulted in an acidic (pH <2), sulfur-rich fumarole system (Hurwitz et al., 2003). This proximity to the primary magmatic system below the volcano has resulted in a magmatic fumarole system dominated by large, ~2 m high, white-tan mounds that emit sulfurous gases and contain large native sulfur crystals (Hughes et al., 2019).

2.2.2 Kilauea Iki

Kilauea Iki erupted in 1959, opening fissures from which lava fountains erupted up to ~600 m in the air and flowed into a pit crater to form a lava lake (Garcia et al., 2003; Stovail, 2009). Spatter and scoria from the eruption formed a ~70 m tall tephra cone (Neal and Lockwood, 2003). The basalts of this eruption are picritic, with an average of ~15 wt. % MgO (Richter and Moore, 1966; Garcia et al., 2003)

The fumaroles found on Kileaua Iki are sourced from meteoric groundwater with a near neutral pH of ~6.5 and have no evidence of sulfur to indicate mixture with magmatic gases (McMurtry et al., 1977).

2.2.3 Mauna Ulu

Mauna Ulu is a parasitic shield volcano that erupted from 1969-1971. The eruption consisted of lava fountaining and built a 50 m tephra cone with a lava lake in the summit, followed by a period of effusive lava flows (Swanson et al., 1979).

Fumaroles on Mauna Ulu are meteoric and appear near the summit rim, the lower west flank where the MU lavas flowed over and filled the ʻĀloʻi pit crater, and on the east flank, all of which lie along the east rift zone (ERZ) (Swanson et al., 1979; Hughes et al., 2019). On the south flank of MU we sampled relict fumarole and syn-emplacement material. This flank exhibited no active fumarole activity at the time of our field work.

2.3 Basalt Alteration

Alteration of basaltic rocks occurs when gases and/or liquids change the original mineralogy and/or physical properties of the rock. Various hydrological processes can alter basalt either syn- or post-emplacement. Syn-emplacement alteration can occur either when volatiles contained in the lava exsolve (intrinsic) during emplacement, or when lava comes into contact with external water such as wet ground (extrinsic). In this work, we consider intrinsic syn-emplacement alteration in which volatiles were concentrated within blisters near lava flow surfaces. Post-emplacement alteration occurs after the lava has solidified. One example of post-emplacement alteration is hydrothermal alteration by fumaroles. Fumaroles are the surface manifestation of subsurface hydrothermal systems and may include meteoric and magmatic water sources, both of which are included in this work.

2.3.1 Post emplacement alteration

Magmatic fumaroles are the result of volcanic volatiles and elements such as H_2O, CO_2, F, Cl, S, and/or P mixing with hot meteoric water resulting in a low pH (<2) system (Hurwitz et al., 2003). These fumaroles result in a variety of alteration products that range from precipitation of minerals to the formation of clays. Magmatic hydrothermally altered basalts are tan-yellowish in color and significantly enriched in SiO_2 and TiO_2, with depletion of all other major element oxides (Payne and Mau, 1946). The rock is characterized by opal, small amounts of kaolinite or related clay minerals, and sulfur crystals present in vesicles (Macdonald, 1944). Magmatic hydrothermal systems on Kilauea exhibit amorphous silica encrustations as well as Al-, Fe-, Mg-, and Ca- sulfates within and on plagioclase- and olivine-rich basalts (Golden et al., 2005). The silica encrustations can contain Fe-Ti oxides and grow at a rate of 1-5 μm/year (Chemtob and Rossman, 2014). The alteration to silica occurs post-emplacement and forms as a result of *in situ* dissolution-precipitation of silica (Chemtob and Rossman, 2014). This process occurs in acidic hydrothermal systems containing F^-, which helps solubilize the silica for transport and precipitation at the surface (Naughton et al., 1976; Chemtob and Rossman, 2014).

Meteoric fumaroles are characterized by near-neutral pH (6.5 – 7.0) hydrothermal waters derived from groundwater (McMurtry et al., 1977). Alteration products formed during experimental alteration at 45° and 70º C in meteoric hydrothermal systems include amorphous silica, smectite clays, and kaolinite that can absorb other elements that are released during alteration of basalt (Gislason and Eugster, 1987; Gislason et al., 1993). In contrast to magmatic fumaroles, meteoric fumaroles were associated with a decrease in SiO_2 and MgO, and an increase in Al_2O_3 (Payne and Mau, 1946).

2.3.2 Syn-emplacement alteration

Syn-emplacement alteration occurs when high temperature volcanic gases exsolve from a lava and cause rapid oxidation of the newly forming rocks, turning them bright red, yellow, orange, and purple (Hughes et al., 2019). In the high temperature oxidizing environment of syn-emplacement volatile degassing, olivine may undergo exsolution of iron oxides in the mineral (Baker and Haggerty, 1967).

In order to better understand where we might find evidence of past life on Mars, we need to better understand the spatial gradients and alteration products associated with a variety of water-rock interactions on Earth. Previous research on hydrothermal basalt alteration gives us insight into what we can expect to find on and/or within the basalts. However, it has not focused on the degree nor the spatial distribution of alteration a rock has undergone within a fumarolic system. Additionally, previous work has not compared the types of alteration products resulting from differing modes of water-rock interaction (e.g., magmatic vs. hot meteoric fumaroles vs. syn-emplacement).

Chapter 3: Manuscript

3.1 Introduction

Understanding how basaltic terrains change as a result of interaction with hydrothermal systems both syn- and post-emplacement is important for Mars exploration because it has been hypothesized that life on Earth began in hydrothermal systems associated with basaltic volcanism (Horneck, 2000; Konhauser et al., 2002; Walton, 2008; Djokic et al., 2017; Damer and Deamer, 2020). Water-rock interaction has the potential to change the mineralogy and geochemistry of the rock. This is important to the search for extraterrestrial life, which may occur as endolithic microbes, as these changes potentially make the rock more or less habitable (Horneck, 2000; Al-Hanbali et al., 2001; Varnes et al., 2003). Understanding the mineralogical and geochemical changes that are caused by different warm water and basalt reactions and their spatial scales are important steps toward searching for past life on Mars.

Mars is within the habitable zone of the sun, making it a key target in NASA's search for life outside of our planet. While Mars is currently dry and cold, it may have been relatively warm and wet during the Noachian and Hesperian periods (4.1 – 2.9 Ga) and had active volcanism (Pollack et al., 1987; Craddock and Howard, 2002; Vago et al., 2017). These conditions could have created habitable conditions for endolithic microbial communities that would have utilized hydrothermally altered basalt for energy and nutrients (Dunfield and King, 2004; Costello et al., 2009; Callac et al., 2013; Cockell et al., 2013, 2019). While these living communities have been hypothesized for Mars, we currently do not know which water-rock alteration states would have offered the best chances for microbial habitability, and, therefore, do not know which rocks to target for closer investigation in search of evidence of past life.

In order to further explore potential habitable environments on Mars, we examined the mineralogy and geochemistry of lavas from three different Kilauean eruptions, including five hydrothermal alteration styles: active and relict magmatic fumaroles on the Kilauea caldera floor (KK), relict meteoric fumaroles at Kilauea Iki (KI), and active and relict meteoric fumaroles and syn-emplacement alteration at Mauna Ulu (MU). The work was carried out as part of the NASA BASALT (Biologic Analog Science Associated with Lava Terrains) research program by an interdisciplinary team of scientists investigating the changes in rocky substrate and associated microbial communities in a Mars analog system (Cockell et al., 2019; Hughes et al., 2019; Lim et al., 2019); this paper reports on the mineralogical and geochemical patterns in alteration observed at the Hawaiian field sites.

3.2 Background

3.2.1 Mars

Volcanism on Mars dominated by tholeiitic basalt erupted as volcanic plains of effusive lava flows, episodes of shield building (e.g. Olympus Mons), steep-sided domes (e.g. Tharsis Tholus), and cinder cones (e.g. Ulysses Colles), resulting in terrain similar to that of Kilauea, Hawai'i (Greeley and Spudis, 1981; Wilson and Head, 1983; Sigurdsson et al., 1999). Kilauea has been used as a martian analog site in the past due to its geochemical morphologic similarity (Greeley, 1974; Konhauser et al., 2002; King and McLennan, 2010; Ruff et al., 2011; Chemtob and Rossman, 2014; Sun and Milliken, 2019).

The martian surface is predominantly composed of basalt in the southern highlands and weathered basalt in the northern lowlands (Bandfield, 2000; Wyatt and McSween, 2002). Chemically, martian basalts have ~16 – 21 wt.% Fe_2O_3* and ~0.5 – 2 wt.% TiO_2 (Greeley and

Spudis, 1981; Bridges and Warren, 2006). Thermal Emission Spectrometer (TES) data from the Mars Global Surveyor and Thermal Emission Imaging System (THEMIS) indicate that, compositionally, martian basalts in the Ganges and Eos Chasma region of the Valles Marineris and Ares Vallis are olivine enriched with 12 - >15% olivine as ~Fo_{68-80} (Morris et al., 2000; Edwards et al., 2008; Ehlmann and Edwards, 2014).

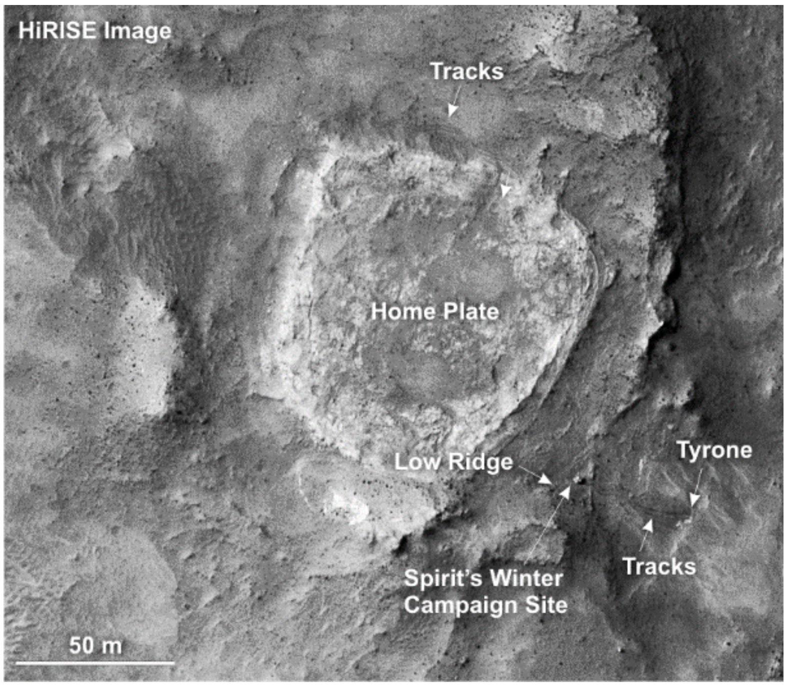

Figure 3: Home Plate in located in the Columbia Hills inner basin. Figure and annotations: NASA/JPL/University of Arizona

The Mars rover Spirit detected high silica rocks and soils at Home Plate, located in the Gusev Crater, that are consistent with opaline silica (Squyres et al., 2008) (Figure 3). The Mars rover Opportunity located a silica-sulfate rich outcrop at Miridiani Planum, located near the equator and on the other side of Mars from the Gusev Crater (Glotch and Bandfield, 2006). The Compact Reconnaissance Imaging Spectrometer (CRISM) and High-Resolution Imaging Science Experiment (HiRISE) instruments located hydrated silica around the Nili Patera caldera within the Syrtis Major caldera complex, suggesting that these deposits were a result of a volcanic hydrothermal system (Skok et al., 2010). River channels, rounded cobbles, phyllosilicates, and the confirmation of opal on Mars are indicators of past surface water and hydrothermal systems

(Baker, 2001; Squyres et al., 2008; Skok et al., 2010; Ruff et al., 2011; Ehlmann and Edwards, 2014).

3.2.2 Kilauea

The BASALT project uses Kilauea as an analog for Noachian-Hesperian martian conditions. Kilauea is situated in warm, wet environment, and is composed of young lavas, 70% of which are < 500 years old (Holcomb, 1987). Tholeiitic basalts from Kilauea are similar to those found on Mars and are primarily composed of Ca-plagioclase, Mg-olivine, and clinopyroxenes and contain ~12 – 15 wt.% Fe_2O_3 and ~ 2.5 – 3.5 wt.% TiO_2 (Sun et al., 1979; Wolfe and Morris, 1996; Sigurdsson et al., 1999; Heltz et al., 2014). The olivine content in Kilauean basalts is Fo_{70-87}, making up ~ 2 – 7% of the rock by volume (Peck et al., 1966; Heltz et al., 2014). Hydrothermal activity on Kilauea consists of hot springs and fumaroles and has resulted in encrustations of amorphous opal on some rocks (Chemtob and Rossman, 2014). The presence of these hydrothermal systems and alteration products, and its legacy as a Mars analog location, make Kilauea a good Mars analog for this study.

While the Kilauea caldera floor (KK) basalts are polygenetic and composed of a number of lava flows of different ages dating back to 1820 CE (Garcia et al., 2003; Duffield et al., 1982), the specific lava flow we studied was emplaced in August 1971. KK lies above the primary magma chamber, and fumaroles in this system are dominated by large, ~2 m high, white-tan solfataric mounds (Hughes et al., 2019). Summit fumaroles near the Halema'uma'u crater have carbon and sulfur isotopes that indicate magmatic origin, and oxygen and deuterium isotope signatures that correspond with meteoric waters, indicating mixing of groundwater with magmatic gases to create the acidic fumarole system (pH <2) (Hurwitz et al., 2003).

Kilauea Iki (KI), a monogenetic eruption consisting of fire fountains, effusive flows into a pit crater, and tephra cone building, erupted in 1959 (Neal and Lockwood, 2003; Garcia et al., 2003; Stovail, 2009); samples here were collected from the cooled lava lake. The fumaroles found on KI are sourced from meteoric groundwater and have no evidence of sulfur to indicate current or prolonged past mixture with magmatic gases. Groundwater on the Big Island of Hawai'i has a near neutral pH of ~6.5, which includes waters sourcing KI and Mauna Ulu fumaroles (McMurtry et al., 1977). The fumaroles of KI appear as slightly reddened basalt around a vent with steam temperatures above 30ºC (Hughes et al., 2019).

Mauna Ulu (MU), a monogenetic, parasitic shield volcano, erupted along the East Rift Zone in 1969 - 1974 with lava fountaining followed by effisive flows (Swanson et al., 1979; Hughes et al., 2019). Fumaroles on MU use meteoric water and follow the spatial trend of the East Rift Zone (ERZ). They are particularly pronounced on the lower west flank where the MU lavas flowed over and filled the ʻĀloʻi pit crater, resulting in a white ring of fumarolic alteration ~200 m diameter and visible in satellite imagery (Swanson et al., 1979; Hughes et al., 2019).

3.2.3 Basalt Alteration

Various processes can alter basalt either during or after emplacement. Syn-emplacement alteration can be the result of intrinsic or extrinsic volatiles; this study focuses on intrinsic syn-emplacement alteration in which high temperature volatiles exsolving from the lava are concentrated within blisters near flow surfaces and oxidize the surrounding rock. Extensive magmatic and meteoric hydrothermal systems on Kilauea alter basalts post-emplacement and change the chemistry and mineralogy of the original basalt. Post-emplacement alteration can occur through many different processes acting after a lava flow has solidified; in this study, however, we focus on the effects of magmatic and meteoric fumaroles.

Magmatic fumaroles are the result of volcanic volatiles mixing with hot meteoric water resulting in a low pH (<2) system (Hurwitz et al., 2003). Hawaiian basalts altered by magmatic fumaroles are tan-yellowish in color and significantly enriched in SiO_2 and TiO_2, with depletion of all other major element oxides (Payne and Mau, 1946), and contain opal, small amounts of kaolinite or related clay minerals, and sulfur crystals (Macdonald, 1944). Acid-sulfate leaching in lab experiments produces amorphous silica from both plagioclase- and olivine-rich basalts, in addition to Al-, Fe-, Mg-, and Ca- sulfates (Golden et al., 2005). The amorphous silica coatings found on the basalts can contain Fe-Ti oxides and grow ~ 1-5 μm/year (Chemtob and Rossman, 2014). (Chemtob and Rossman, 2014). The alteration to silica occurs post-emplacement and forms as a result of *in situ* dissolution-precipitation of silica in acidic hydrothermal systems containing F^-, which helps solubilize the silica (Naughton et al., 1976).

Meteoric fumaroles are characterized by near-neutral pH (6.5 – 7.0) hydrothermal waters derived from groundwater (McMurtry et al., 1977). Alteration products formed during experimental alteration at 45º and 70º C in meteoric hydrothermal systems include amorphous silica, smectite clays, kaolinite that can absorb other elements that are released during alteration of basalt (Gislason and Eugster, 1987; Gislason et al., 1993). In contrast to magmatic fumaroles, meteoric steam vents are associated with a decrease in SiO_2 and an increase in Al_2O_3 (Payne and Mau, 1946).

Syn-emplacement alteration occurs when high temperature volcanic gases exsolve from a lava and causes rapid oxidation of the newly forming rocks, turning them bright red, yellow, orange, and purple (Hughes et al., 2019). In the high temperature oxidizing environment of syn-emplacement degassing of volatiles, olivine may undergo exsolution of iron oxides in the mineral (Baker and Haggerty, 1967).

While this previous research on basaltic alteration and more specifically hydrothermal basalt alteration gives us insights of what we can expect to find, it has focused on neither the degree nor spatial distribution of alteration a rock has undergone within a fumarolic system (e.g., magmatic vs. hot meteoric fumaroles vs. syn-emplacement), nor the relationship between these physical gradients and microbial inhabitation. In order to better understand where we might find evidence of past life on Mars, we need to better understand the spatial gradients and alteration products associated with a variety of water-rock interaction at hydrothermal systems on Earth.

3.3 Methods

3.3.1 Sample Collection

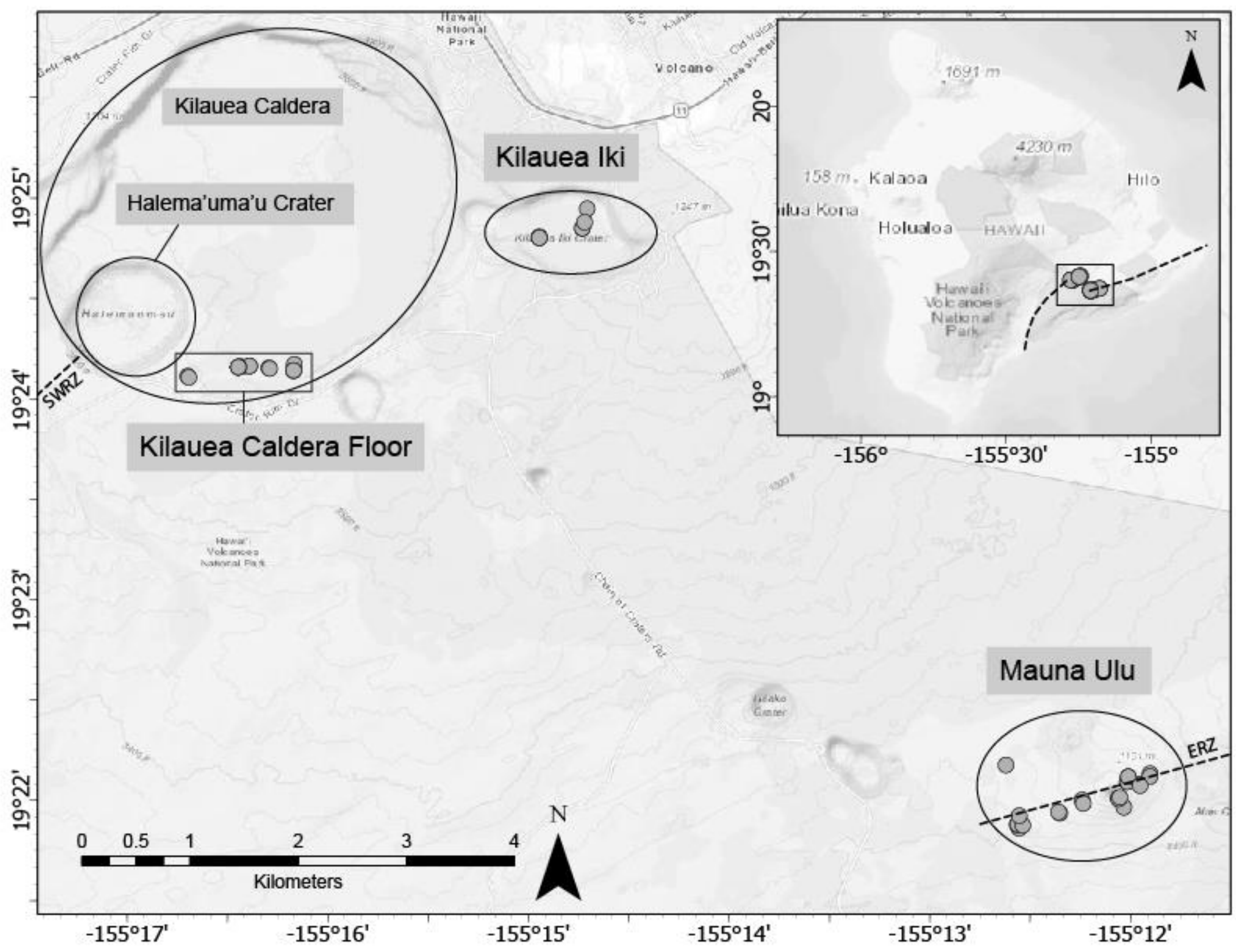

Figure 4: Location of study area showing the Big Island of Hawai'i (inset) and locations of flows sampled and sample locations (gray circles). Basemap sources: Esri, HERE, Garmin, Intermap, increment P Corp., GEBCO, USS, FAO, NPS, NRCAN, GeoBase, IGN, Kadaster NL, Ordnance Survey, Esri Japan, METI, Esri China (Hong Kong), © OpenStreetMap contributors, and the GIS

Basalt samples representing different alteration conditions were collected from the shallow subsurface up to 0.5 m deep from multiple lava flows at MU, KI, and KK (Figure 4 & Table 2), during the NASA BASALT Mars field deployments in 2016 and 2017. The presence of visible alteration varied between the three lava flows included in this study. Alteration styles were categorized *in situ* as unaltered (U); syn-emplacement (SE) altered (only collected at MU);

magmatic and meteoric relict fumaroles (RF); and magmatic and meteoric active fumaroles (AF). Active fumaroles were determined based on the presence of visible steam escaping vents and *in situ* temperature measured using a hand-held forward-looking infrared (FLIR) thermometer and a meat thermometer. Active fumaroles were designated as high temperature (AF-HT) above 80ºC or low temperature (AF-LT) between 60ºC - 80ºC. The high temperature fumarole sites were selected based upon the upper temperature limit for microbial life on Earth being approximately 121ºC (Kashefi and Lovley, 2003). Fumarolic activity with temperatures < 60ºC or no active steam coming out of vents were designated relict fumaroles. Much of the material collected at the active and relict magmatic fumaroles at KK was mantled by up to a half meter of clays and precipitates including native sulfur and silica. The native sulfur precipitates included individual crystals larger than 2 cm across, which were not included in the lab analyses. We had to dig beneath these precipitates in order to find whole rock material that was adequately hot for the high-temperature threshold and solid enough for processing and analyses. All samples collected from KI were from relict fumaroles or unaltered rock, as there were no active fumaroles present on that flow. Ultimately, only a few samples were collected from KI due to the overall lack of alteration present. Alteration types at MU were classified based on measured *in situ* temperature and the presence of steam, red discoloration, and white precipitates within vesicles. While all fumaroles on Earth are presumed to include significant meteoric water due to the presence of groundwater, we consider sulfur smell and the presence of sulfur precipitates as the threshold for classifying a particular fumarole as magmatic.

Table 2: Sample collection locations.

Sample	Alteration	Lat	Long
Kilauea Caldera Floor			
B17-100	U	19.40285884	-155.26944548
B17-011	AF-HT	19.40256298	-155.27156216
B17-25	AF-HT	19.40187840	-155.27830070
B17-172	AF-HT	19.40265196	-155.27383533
B17-310	AF-HT	19.40263000	-155.27409000
B17-158	AF-LT	19.40272000	-155.27316000
B17-180	AF-LT	19.40250981	-155.27149440
B17-195	AF-LT	19.40272000	-155.27316000
B17-095	RF-HD	19.40263000	-155.27409000
B17-392	RF-HD	19.40234597	-155.26951621
B17-170	RF-LD	19.40263000	-155.27409000
B17-391	RF-LD	19.40234042	-155.26950237
B17-020	RF	19.40263000	-155.27409000
B17-066	RF	19.40263000	-155.27409000
B17-377	RF	19.40235354	-155.26950497
B17-75	AF	19.40177027	-155.27820389
Kilauea Iki			
B17-114	U	19.41577694	-155.24512582
B17-152	RF-HD	19.41415655	-155.24552633
B17-338	RF-HD	19.41337821	-155.24910486
B17-362	RF-HD	19.41337749	-155.24910447
B17-168	RF-LD	19.41416190	-155.24552666
B17-339	RF-LD	19.41344233	-155.24909582
B17-357	RF-LD	19.41337749	-155.24910447
B17-295	RF	19.41465314	-155.24534140
B17-376	RF	19.41336797	-155.24909473
Mauna Ulu			
100108	U	19.36887770	-155.19837130
100059	U	19.36670037	-155.20403320
100704	U	19.36609215	-155.20055000
53	U	19.36960000	-155.21034000
100068	AF	19.36435013	-155.20926080
100079	AF- HT	19.36466024	-155.20941690
100093	AF-LT	19.36560047	-155.20587010
100100	AF-HT Halo (100079)	19.36466744	-155.20937310
100126	AF-LT Halo (100718)	19.36821084	-155.20028630
100718	AF-LT	19.36820705	-155.20027700
100040	RF	19.36459886	-155.20895580
100140	RF	19.36862734	-155.20018230
100607	RF	19.36804878	-155.19923240
100700	RF	19.36687939	-155.20100000
100130	RF	19.36539000	-155.20924000
100061	SE	19.36861544	-155.20018280
100070	SE	19.36569670	-155.20598030
100117	SE	19.36864621	-155.19837840
100611	SE	19.36789058	-155.19920920
100729	SE	19.36677493	-155.20099956
100052	SE	19.36641345	-155.20392530
100736	SE	19.36691682	-155.20088422

3.3.2 Sample Processing

Billets for petrographic work were cut using a water-cooled saw, followed by washing in RO water with a stainless steel brush to remove surficial soils and clays and any possible contaminants from billet cutting. After cleaning, the remaining rocks were dried in an oven at 100ºC for 8 hours prior to crushing and powdering via a shatterbox with tungsten rings for whole rock XRF analyses. All equipment used in the cleaning, drying, and powder processing was cleaned between samples using isopropyl alcohol 90 and Kimwipes to avoid cross contamination.

3.3.3 Analyses

We conducted point counts to evaluate the mineralogy of the rock samples, counting 1000-1400 points per slide based on Van der Plas and Tobi (1965) to ensure statistically valid results within 2σ. Phenocrysts were designated as unaltered, partially altered, and completely altered. Unaltered phenocrysts showed no alteration; partially altered phenocrysts were altered along rims and fractures; and completely altered phenocrysts exhibited > 80 % alteration. All counts were normalized to solid rock. Whole rock geochemistry for major element oxides (wt. %) and trace elements (ppm) was conducted by the Christiansen lab at Brigham Young University using a Rigaku ZSX Primus wavelength dispersive X-ray fluorescence (XRF) spectrometer with a rhodium tube and operating at 50kV and 50mA. Scanning Electron Microscopy / Energy Dispersive X-Ray Spectroscopy (SEM/EDS) analyses were conducted at Idaho State University on a Bruker SEM and Bruker Quantax EDS using carbon coated thin sections. EDS element maps were created to illustrate the distribution of elements within a sample and provide information about small-volume precipitates found in vesicles and fractures within the rock. Areas of interest were selected during petrographic work based on precipitates and alteration products visible at a microscopic scale. Combined, these techniques allowed us to evaluate the differences between the unaltered and altered rocks in each area and to develop a nuanced view of the processes involved in each.

3.4 Results

3.4.1 Kilauea Caldera Floor: Magmatic Fumaroles

3.4.1.1 Petrography

Hand samples of material from the KK magmatic fumaroles exhibit a high degree of alteration. The rocks are gray to off-white to yellow in color, with very little dark basalt remaining; that the material was originally basalt and not entirely a secondary precipitate mound is evidenced by the presence of groundmass and phenocryst textures preserved in the rock. In the

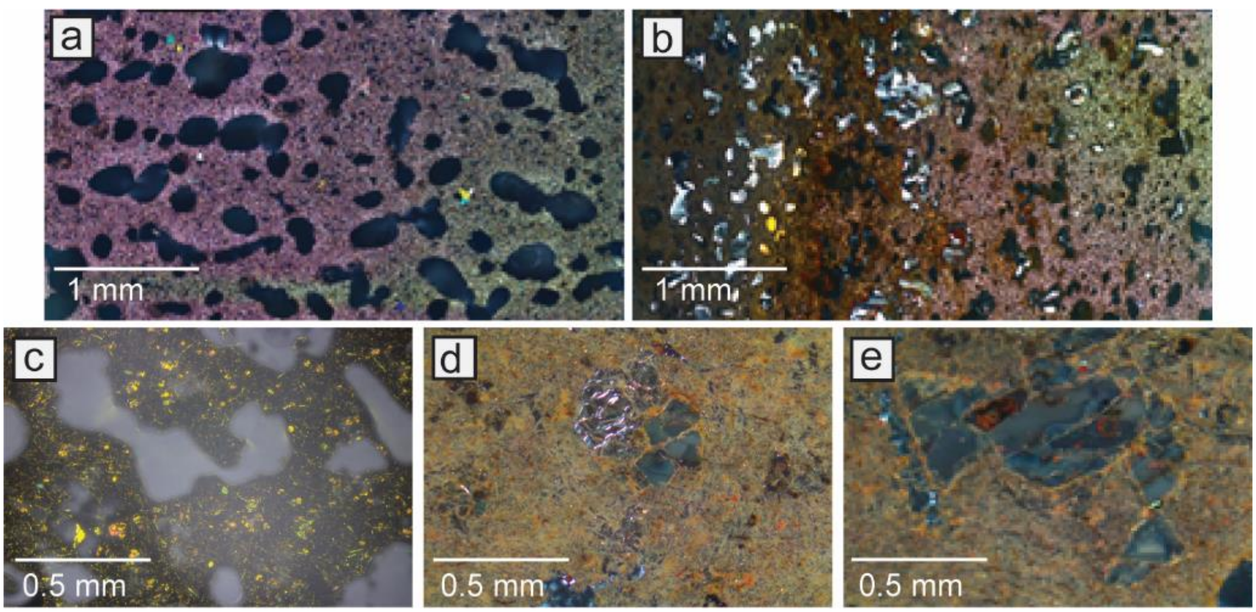

Figure 5: Photomicrographs from the Kilauea caldera floor showing degrees of alteration (all in XP). a) unaltered; b) active fumarole – low temp c) relict fumarole showing silica precipitation in vesicles and alteration of olivine to iddingsite on rims and in fractures; d) opalized phenocryst from a low temperature active fumarole; e) different style opalized phenocryst from a low temperature active fumarole.

field, these rocks are covered by layers of amorphous silica, native sulfur, and clays with a total maximum thickness of 0.5-1 m. The groundmass and phenocrysts within high temperature samples are completely altered, with some of the original phenocryst outlines still present but none of the optical properties of the original minerals. The low temperature active fumaroles are less altered and display varying degrees of alteration within a single sample (Figure 5b). Relict fumarole alteration is highly variable, from minimal alteration to nearly complete mineral and groundmass replacement (Figure 5). Petrographic analysis of KK samples shows varying degrees of alteration, with a positive correlation between recorded field temperature and degree of alteration. However, one low temperature fumarole and four relict fumarole samples exhibit the same degree of alteration, which we interpret to indicate that these may have previously been active, high-T fumaroles.

Petrographic microscope observations indicate that KK magmatic fumarole alteration products appear to be a heterogeneous mixture of SiO_2 and other major element oxides that we were unable to identify using petrographic techniques. While damp clays were observed overlying the rocks in the fumarole mounds, the altered basalts did not contain evidence of alteration to clays within the rock matrix itself. While clay would have been removed from the billet surface during the cleaning process, we interpret the total dearth of clay in the rock to be the result of removal during breakdown of the protolith by rising hot, acidic water.

The unaltered sample collected from KK contains 5 ± 2% phenocrysts and 95 ± 2% groundmass, normalized to vesicle free solid rock (Table 3). The unaltered sample contains minor amounts of partially altered olivine (0.3 ± 0.2 %) and pyroxene (0.1 ± 0.1%) and two completely altered olivine phenocrysts (0.3 ± 0.4 %).

Low temperature active fumaroles and relict fumaroles that are not completely altered still resemble basalt and are not the white-yellow color seen in the highly altered specimens. Partially altered phenocrysts account for a mean 4 ± 1% of solid rock in the form of plagioclase (8 ± 2 %), olivine (5 ± 2%), and pyroxene (1.5 ± 0.9 %). Mean completely altered olivine accounts for 5 ± 2 % and pyroxene for 18 ± 3 % of solid rock. Iddingsite alteration of olivine and pyroxene crystals is the predominant mineral alteration seen in these samples. Non-normalized data shows that these low temperature and active fumaroles contain 4 ± 1% layered amorphous silica and opaque vesicle fill.

The highly altered KK samples contain a mean 97 ± 4% amorphous opal (counted as groundmass and opal) and normalized to vesicle free solid rock (Table 3). Unaltered olivine accounts for a mean 0.6 ± 0.5% of the solid rock. Partially altered olivine comprises ~ 0.6 ± 0.5% of the solid rock, and completely altered phenocrysts that are unidentifiable make up ~7 ± 2% of the solid rock. Non-normalized data shows that vesicle fill by native sulfur and white, amorphous stalagmite-like precipitates account for a mean of 3 ± 1% of the whole rock (including void space).

The remaining samples are completely altered and only the original shape of phenocrysts exists at a microscopic level. These rocks are off-white to yellow in color with no visible phenocrysts. Vesicles contain growths of native sulfur and amorphous silica. The groundmass is a gold/brown color in XP and a mixture of opaque material and colorless plagioclase lathe outlines in PPL. Although the shapes of the phenocrysts are still visible in the highly altered samples, they retain none of their original optical properties and appear as a filmy grayish color in XP, with a few showing light purple opalescence in XP. The highly altered samples are 100% amorphous opal (Figure 5d, e).

Table 3: Point count data from Kilauea caldera floor normalized to vesicle free (solid rock %), non-normalized (whole rock %) and standard deviation within 2σ. U = Unaltered; PA = Partially altered; CA = Completely altered; Unk = Unknown

	B17-100	U		B17-25	AF - HT		B17-180	AF - LT		B17-195	AF - LT		B17-349	RF		B17-170	RF	
	solid rock %	whole rock %	2σ	solid rock %	whole rock %	2σ	solid rock %	whole rock %	2σ	solid rock %	whole rock %	2σ	solid rock %	whole rock %	2σ	solid rock %	whole rock %	2σ
Vesicles		28.4	2.9		28.5	2.9		17.7	2.4		18.3	2.4		31.7	2.9		10.6	1.9
Groundmass	94.9	66.5	1.7	99.3	69.9	0.6	33.7	21.6	3.7	69.0	46.6	3.6	90.7	46.8	2.6	58.7	51.5	3.3
Plagioclase - U	2.7	1.9	1.2	0.0	0.0	0.0	0.5	0.3	0.5	4.0	2.7	1.5	0.0	0.0	0.0	0.0	0.0	0.0
Plagioclase - PA	0.0	0.0	0.0	0.0	0.0	0.0	0.0	0.0	0.0	14.1	9.5	2.7	2.1	1.1	1.3	0.0	0.0	0.0
Olivine - U	1.4	1.0	0.9	0.0	0.0	0.0	0.0	0.0	0.0	0.6	0.4	0.6	0.0	0.0	0.0	0.6	0.5	0.5
Olivine - PA	0.3	0.2	0.4	0.0	0.0	0.0	0.5	0.3	0.5	11.3	7.6	2.4	4.8	2.5	1.9	0.1	0.1	0.2
Olivine - CA	0.3	0.2	0.4	0.0	0.0	0.0	0.0		0.0	0.0	0.0	0.0						
Pyroxene - U	0.3	0.2	0.4	0.0	0.0	0.0	0.0	0.0	0.0	0.0	0.0	0.0	0.0	0.0	0.0	0.0	0.0	0.0
Pyroxene - PA	0.1	0.1	0.3	0.0	0.0	0.0	0.0	0.0	0.0	1.0	0.7	0.8	1.7	0.9	1.2	0.0	0.0	0.0
Pyroxene - CA	0.0	0.0	0.0	0.0	0.0	0.0	0.0	0.0	0.0	0.0	0.0	0.0						
Unk phenocryst - CA	0.0	0.0	0.0	0.7	0.5	0.6	0.0	0.0	0.0	0.0	0.0	0.0						
Opal	0.0	0.0	0.0	0.0	0.0	0.0	65.4	41.9	3.8	0.0	0.0	0.0	0.6	0.3	0.7	40.7	35.7	3.3
Vesicle fill - yellow		0.0	0.0		0.6	0.5		3.7	1.2		0.1	0.2		12.9	2.1		0.0	0.0
Vesicle fill - opaque		1.5	0.8		0.5	0.4		5.2	1.4		11.7	2.0		1.8	0.8		0.8	0.6
Vesicle fill - clear		0.0	0.0		0.0	0.0		9.3	1.8		2.4	1.0		2.0	0.9		0.8	0.6

	B17-75	AF-LT		B17-158	AF-LT		B17 - 348	RF		B17 - 392	RF		B17-377	RF	
	solid rock %	whole rock %	2σ	solid rock %	whole rock %	2σ	solid rock %	whole rock %	2σ	solid rock %	whole rock %	2σ	solid rock %	whole rock %	2σ
Vesicles		19.3	2.5		23.2	2.7		36.0	3.0		32.5	3.0		39.4	3.1
Groundmass	86.4	67.2	2.5	51.5	36.7	3.7	93.7	41.9	2.3	92.5	57.2	2.1	99.0	56.7	0.9
Plagioclase - U	0.0	0.0	0.0	3.7	2.6	1.4	0.0	0.0	0.0	1.0	0.6	0.8	0.0	0.0	0.0
Plagioclase - PA	0.0	0.0	0.0	0.0	0.0	0.0				0.0	0.0	0.0	0.0	0.0	0.0
Olivine - U	0.0	0.0	0.0	14.0	10.0	2.6	2.7	1.2	1.5	3.6	2.2	1.5	0.0	0.0	0.0
Olivine - PA	0.0	0.0	0.0	0.0	0.0	0.0	2.7	1.2	1.5	0.7	0.4	0.7	1.0	0.6	0.9
Olivine - CA	0.0	0.0	0.0	9.8	7.0	2.2	0.9	0.4	0.9	0.0	0.0	0.0			
Pyroxene - U	0.0	0.0	0.0	0.0	0.0	0.0	0.0	0.0	0.0	0.0	0.0	0.0	0.0	0.0	0.0
Pyroxene - PA	0.0	0.0	0.0	2.8	2.0	1.2	0.0	0.0	0.0	0.5	0.3	0.6	0.0	0.0	0.0
Pyroxene - CA	0.0	0.0	0.0	18.1	12.9	2.9	0.0	0.0	0.0	0.0	0.0	0.0			
Unk phenocryst - CA	13.6	10.6	2.5	0.0	0.0	0.0				0.0	0.0	0.0			
Opal	0.0	0.0	0.0	0.0	0.0	0.0				1.8	1.1	1.1	0.0	0.0	0.0
Vesicle fill - yellow		0.0	0.0		0.4	0.4		6.0	1.5		2.4	1.0		0.0	0.0
Vesicle fill - opaque		2.9	1.1		4.7	1.3		10.4	1.9		3.2	1.1		0.2	0.3
Vesicle fill - clear		0.0	0.0		0.5	0.4		2.9	1.1		0.0	0.0		3.1	1.1

3.4.1.2 Major Element Oxides

The most highly altered specimens from the magmatic fumarole system on the Kilauea caldera floor are dominated by SiO_2 in the form of amorphous opal. The overwhelming enrichment in opal seen in thin section is consistent with XRF results, which indicate that up to 93%, of the rock is now SiO_2. Accounting for bulk normalization, this represents an increase of ~20x and is echoed by a similar increase in TiO_2 (Table 4 & Figure 6). SEM/EDS analyses indicate that both the groundmass and phenocrysts within these samples have been replaced with amorphous opal where the original elements that make up the bulk rock have been removed and silica has filled in the voids. Evidence of this is seen in the SEM/EDS imagery, where outlines of plagioclase in the groundmass and of phenocrysts are evident, but the signature is overwhelmed with Si. EDS element maps display bright clusters of Ti in the groundmass and Fe/Ti in equant dendritic crystals within fractures, which we interpret to be anatase crystals and titanomagnetite, respectively (Figure 7a, b). We infer that low pH waters dissolved SiO_2 and TiO_2 from basalts deeper within the system and precipitated amorphous opal, anatase, and titanomagnetite near the surface as temperatures decreased dramatically.

The depletion patterns for Al_2O_3, Fe_2O_3, MgO, and CaO are very similar to one another (Figure 6Figure 6). While the overall decrease in iron content has been driven by the removal of olivine phenocrysts, SEM/EDS analyses display secondary 30 – 70 μm Fe/Ti-dendrites within fractures near vesicles. Their equant shape and the presence of both Fe and Ti in these dendrites indicate that they are titanomagnetite precipitates (Figure 7b). These dendrites are common near vesicles in highly altered rock. Layered Si/Al precipitates occur as amorphous layered growths within many vesicles (Figure 7c). The relative depletions in MgO and CaO are consistent with the removal of olivine and plagioclase phenocrysts observed in thin section (Table 4).

Table 4: Whole rock XRF for Kilauea caldera floor reported as wt. %. Normalized to 100% Volatile-free with all Fe as Fe_2O_3.

Samples	Alteration	SiO_2	TiO_2	Al_2O_3	Fe_2O_3	MnO	MgO	CaO	Na_2O	K_2O	P_2O_5	Total	LOI
100	U	50.03	2.52	13.20	12.49	0.17	7.59	11.17	2.10	0.48	0.24	100	-0.61
11	HT	89.73	4.64	3.21	1.25	0.01	0.15	0.41	0.06	0.39	0.15	100	6.00
25	HT	91.48	3.67	2.82	0.94	0.01	0.16	0.42	0.05	0.33	0.11	100	4.74
172	HT	92.26	5.06	1.70	0.49	0.01	0.08	0.16	0.00	0.16	0.07	100	11.94
310	HT	93.43	2.91	2.14	0.66	0.01	0.10	0.21	0.06	0.36	0.12	100	5.98
158	HT	58.19	3.13	10.50	11.52	0.12	5.87	8.23	1.53	0.63	0.28	100	5.52
180	LT	71.42	3.74	7.00	7.51	0.07	2.68	5.86	0.92	0.57	0.23	100	6.78
195	LT	54.28	3.03	11.13	11.73	0.13	5.45	11.57	1.77	0.63	0.27	100	7.21
75	LT	90.92	3.80	3.30	0.80	0.01	0.10	0.37	0.11	0.46	0.12	100	5.46
95	RF-HD	90.08	4.23	3.50	0.76	0.02	0.22	0.51	0.07	0.43	0.18	100	15.42
392	RF-HD	62.93	2.91	9.44	9.76	0.11	4.58	7.78	1.65	0.59	0.25	100	3.71
349	RF-HD	65.31	3.78	8.22	12.86	0.11	3.38	4.51	0.83	0.68	0.30	100	5.38
170	RF-LD	81.19	3.88	5.17	3.31	0.05	1.89	3.03	0.70	0.55	0.21	100	4.91
391	RF-LD	90.14	4.37	2.95	1.21	0.01	0.11	0.47	0.17	0.41	0.16	100	5.12
348	RF-LD	67.50	3.77	6.50	16.22	0.07	1.78	2.24	0.84	0.76	0.32	100	8.45
20	RF	58.43	1.92	2.82	1.08	0.02	0.68	34.59	0.01	0.31	0.13	100	16.51
66	RF	49.39	2.56	2.38	0.68	0.02	0.56	44.11	0.00	0.19	0.10	100	13.43
377	RF	90.59	5.01	2.88	0.72	0.01	0.08	0.25	0.00	0.34	0.12	100	5.65

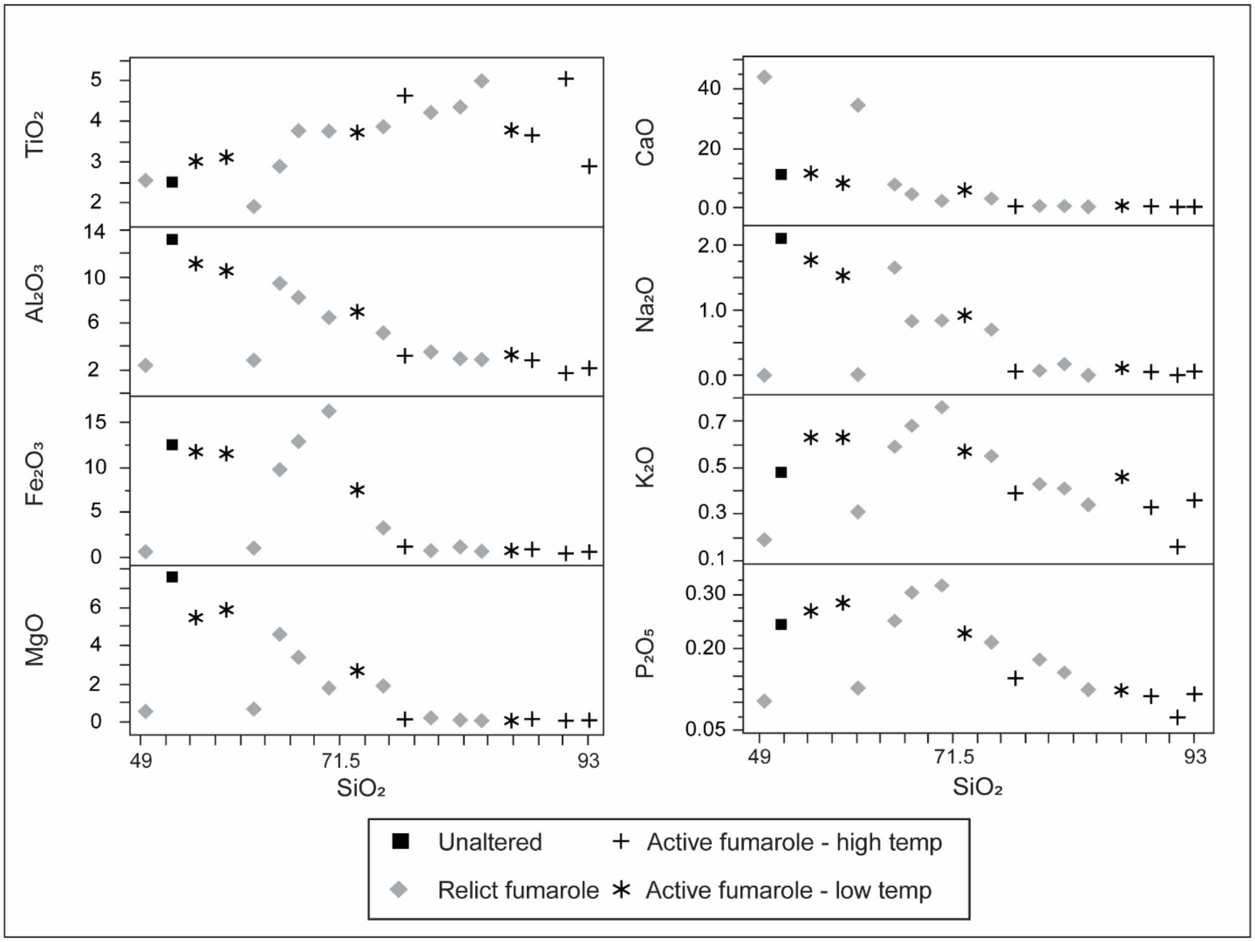

Figure 6: Harker diagrams for KK major element oxides. Note the enrichment in TiO_2 as SiO_2 increases. Al_2O_3, Fe_2O_3, and MgO exhibit very similar depletion patterns with two LT fumaroles decreasing slightly, then a relatively linear depletion trend until the wt% is just above 0.

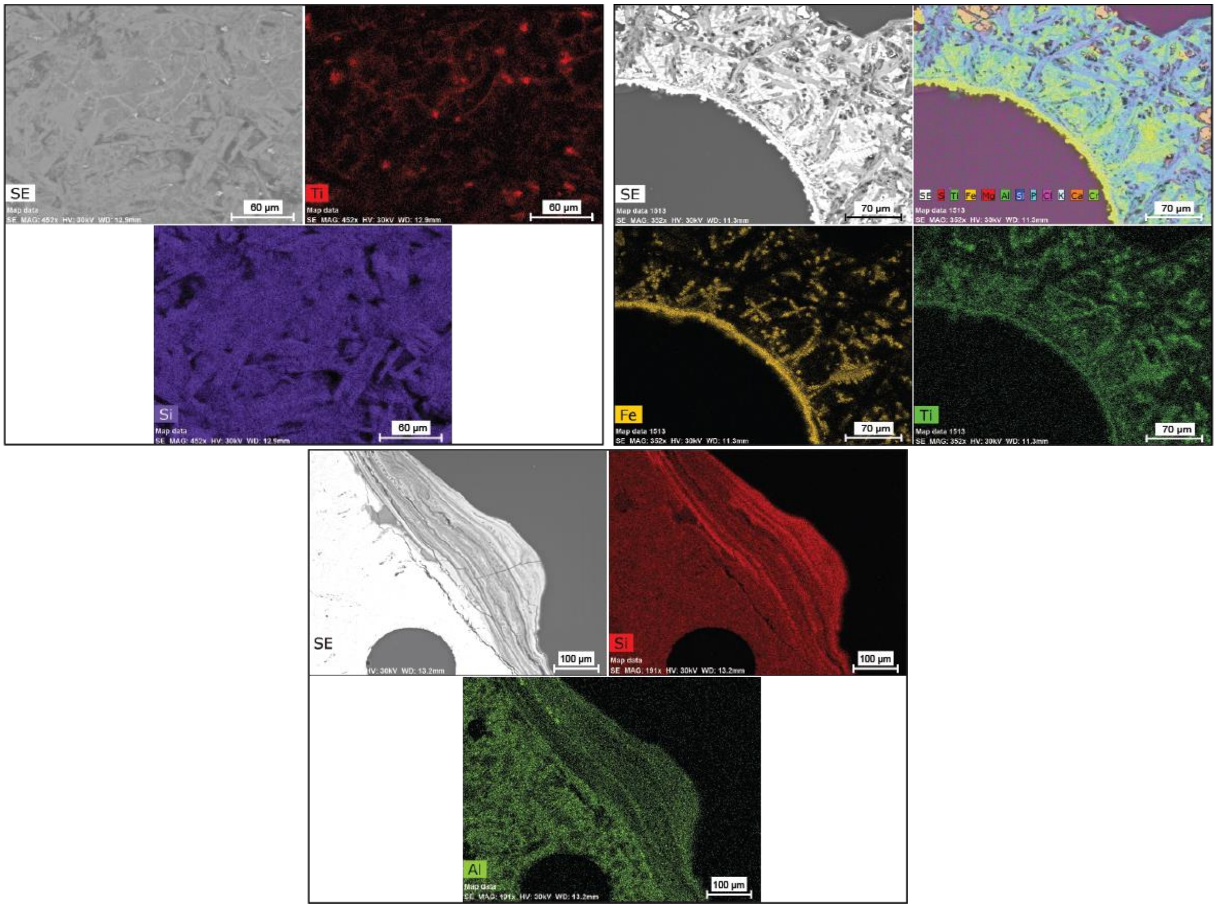

Figure 7: SEM/EDS map of a KK relict fumarole sample (377) showing: a) Plagioclase rich groundmass which has been replaced by Si and Ti; b) Titanomagnetite dendrites within fractures; c) Layered Si-Al vesicle precipitate.

3.4.1.3 Trace Elements

Trace element analyses of the Kilauea caldera floor samples showed notable enrichment in Cl and S, with over half the samples containing >1 wt. % sulfur (Figure 8 & **Error! Reference source not found.**). Sr, V, Cr, Ni, Cu, Zn, Sc, Ga, and Nd were depleted relative to the unaltered sample. Acidic volatiles, including SO_2, H_2S, HF, and/or HCl, rising through the

Kilauea caldera floor fumaroles dissolve and mobilize these elements in solution and deposit them at the surface within the clays, leading to the depletion seen in the rock samples.

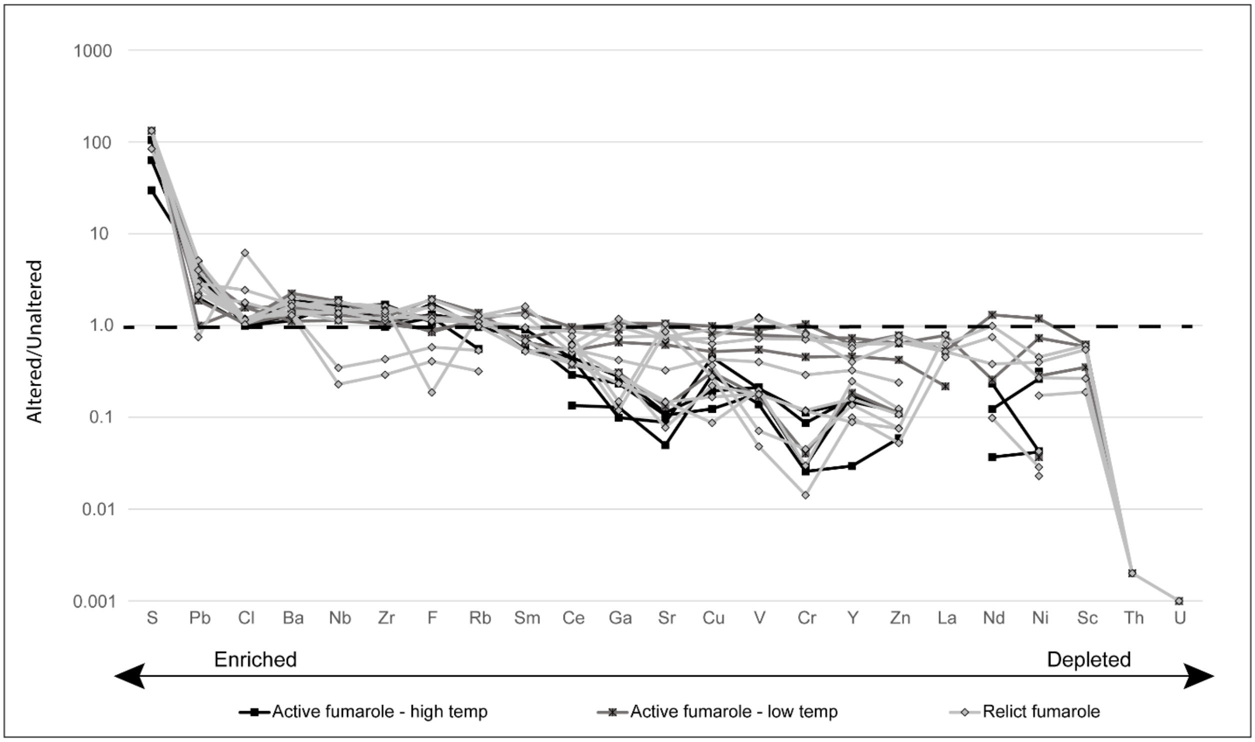

Figure 8: Spider diagram of Kilauea caldera floor trace element concentrations normalized to unaltered and sorted by mean enrichment (highest to lowest). Dashed line indicates unaltered sample. Sulfur exhibits the largest enrichment, followed by Pb and Cl. Values for Th and U were assigned small non-zero numbers (0.002 and 0.001 respectively) based on their mean non-normalized concentrations, due to the inability to normalize to 0 ppm.

Table 5: XRF trace element analyses from magmatic fumaroles associated with the Kilauea caldera floor reported in ppm.

Sample	100	11	25	172	310	75	158	180	195	95	392	349	170	391	348	20	66	377
Alteration	U	HT	HT	HT	HT	HT	LT	LT	LT	RF-HD	RF-HD	RF-HD	RF-LD	RF-LD	RF-LD	RF	RF	RF
S	151	4485	15781	>1 wt %	9551	>1 wt %	>1 wt %	>1 wt %	>1 wt %	>1 wt %	>1 wt %	>1 wt %	>1 wt %	>1 wt %	>1 wt %	>1 wt %	>1 wt %	12694
Sr	352	40	37	18	31	46.3	370	217	370	52	273	247	114	52	264.9	367	303	27
V	326	69	59	45	67	55.2	293	178	258	65	236	401	131	59	390.7	23	16	58
Cr	353	31	11	9	40	14.2	366	161	263	11	250	295	103	42	283	16	5	41
F	177	192	305	217	233	344	150	217	159	288	215	33	339	198	0	103	72	277
Cl	70	74	72	70	71	79	111	73	110	170	81	83	83	73	81	434	125	72
Zr	157	264	166	152	172	193	192	224	162	178	191	245	210	255	231.1	67	46	223
Ni	122	5	5	38	32	4.5	145	34	89	3	55	49	21	4	32.9	0	0	5
Cu	114	22	14	33	51	35.3	112	59	96	10	72	83	49	19	103.7	42	32	25
Zn	105	12	12	6	12	11.7	82	44	67	13	67	81	25	11	69.2	8	6	8
Ba	84	144	106	95	152	187	133	110	93	142	119	111	151	170	121.2	116	108	137
Sc	35	0	0	0	0	0	22	12	21	0	21	19	7	0	9.3	0	0	0
Ga	20	6	5	3	2	6.2	22	13	18	6	15	20	9	5	23.9	3	2	6
Nb	15	25	25	26	29	28.1	20	20	17	22	17	21	24	27	20.9	5	4	28
Ce	32	14	9	4	14	11.9	31	17	30	18	27	16	18	13	20.1	24	20	12
Nd	16	4	1	0	2	0	21	0	4	0	16	6	0	2	12.2	0	0	0
Y	27	4	5	1	4	5	17	13	20	7	17	15	9	4	10.9	4	3	2
La	11	0	0	0	0	0	6	2	9	0	7	6	0	0	5.7	9	5	0
Rb	10	12	10	6	11	13.9	12	12	11	10	11	13	13	11	12.9	5	3	10
Sm	4	2	3	0	4	3	6	3	3	0	4	6	2	3	7.1	0	0	2
Th	0	5	2	3	3	2.8	2	0	0	3	0	0	4	5	0	0	0	4
Pb	1	4	2	3	3	3.7	3	2	1	2	2	2	4	4	2.1	1	2	3
U	0	0	1	0	1	0	0	0	0	0	0	0	0	0	0	0	0	1

3.4.2 Kilauea Iki: Relict Meteoric Fumaroles

3.4.2.1 Petrography

The relict fumaroles at KI exhibit red discoloration and small, white secondary precipitates in vesicles in hand sample but do not appear profoundly altered from the original basalt. Point counts indicate that the unaltered sample contains 7 ± 3% phenocrysts; 6 ± 2% olivine and 1 ± 1% pyroxene, none of which exhibit alteration. Point counts of the relict fumaroles give a mean 5.2 ± 1.8% olivine and 4.6 ± 1.7% clinopyroxene phenocrysts, normalized to solid rock. Unaltered olivine and pyroxene account for a mean 8 ± 3% and 6 ± 2% of the solid rock, respectively (Table 6). Partially altered olivine and pyroxene contribute to a mean of 2.4 ± 1.0% and 2.2 ± 1.3%, respectively. Completely altered olivine accounts for a mean of 2 ± 1% of the solid rock. Mean counts show that 86 ± 3% of the solid rock is tachylite groundmass. Vesicles account for 50 ± 1% of the non-normalized rock, and 4 ± 1% of the vesicles are filled by secondary precipitates (Table 6).

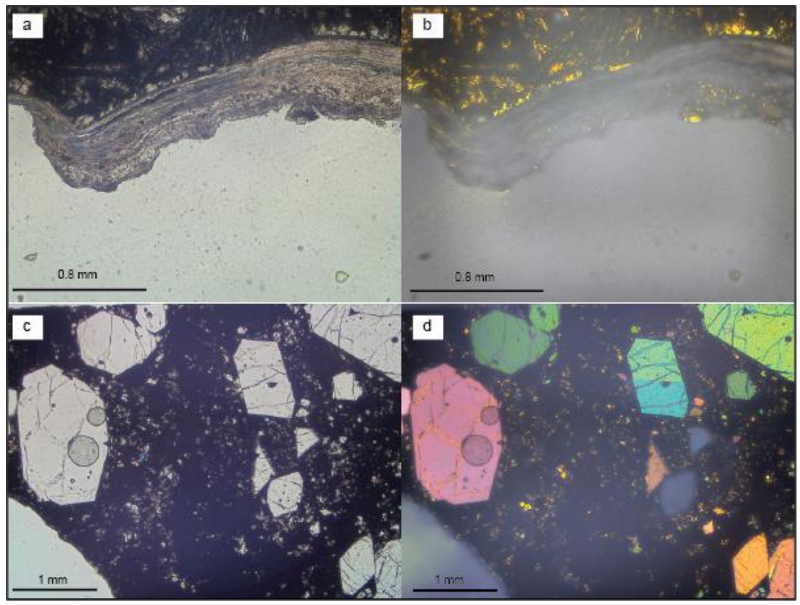

Figure 9: Photomicrographs of Kilauea Iki samples: a) Vesicle precipitation in a high density relict fumarole (152) in ppl (10x); b) The same vesicle precipitation in XP; c) Groundmass and phenocrysts of a relict fumarole (295) in ppl showing a tachylite groundmass and unaltered phenocrysts; d) The same sample in XP.

The alteration of phenocrysts occurs as iddingsite along rims and within fractures in olivine and pyroxene. The precipitates found in the vesicles are similar to those found at KK and appear to be amorphous silica layered with magnesium and small amounts of aluminum (Figure 9). These precipitates are visible in hand samples and microscopy, and they appear as white stalagmite-type growths within vesicles. There is no evidence clay alteration within the matrix of the rocks collected from the relict fumaroles of KI.

Table 6: Point count data from Kilauea Iki normalized to vesicle free (solid rock %), non-normalized (whole rock %) and standard deviation within 2σ. U = Unaltered; PA = Partially altered; CA = Completely altered

	B17-114	U		B17-152	RF		B17-338	RF		B17-339	RF		B17-295	RF	
	solid rock %	whole rock %	2σ	solid rock %	whole rock %	2σ	solid rock %	whole rock %	2σ	solid rock %	whole rock %	2σ	solid rock %	whole rock %	2σ
Vesicles		44.5	3.1		37.9	3.1		39.6	3.1		52.1	3.2		59.5	3.1
Groundmass	93.2	49.0	2.2	95.4	54.5	1.7	74.6	43.5	3.6	68.2	32.1	4.3	90.4	35.6	3.0
Plagioclase - U	0.0	0.0	0.0	0.0	0.0	0.0	0.0	0.0	0.0	0.0	0.0	0.0	0.0	0.0	0.0
Olivine - U	5.5	2.9	2.0	3.0	1.7	1.4	16.3	9.5	3.1	11.9	5.6	3.0	0.0	0.0	0.0
Olivine - PA	0.0	0.0	0.0	0.4	0.2	0.5	0.0	0.0	0.0	0.2	0.1	0.4	1.8	0.7	1.3
Olivine - CA	0.0	0.0	0.0	0.0	0.0	0.0	0.0	0.0	0.0	0.0	0.0	0.0	2.8	1.1	1.7
Pyroxene - U	1.3	0.7	1.0	1.2	0.7	0.9	9.1	5.3	2.4	19.1	9.0	3.6	0.5	0.2	0.7
Pyroxene - PA	0.0	0.0	0.0	0.0	0.0	0.0	0.0	0.0	0.0	0.6	0.3	0.7	4.6	1.8	2.1
Pyroxene - CA	0.0	0.0	0.0	0.0	0.0	0.0	0.0	0.0	0.0	0.0	0.0	0.0	0.0	0.0	0.0
Vesicle fill - yellow					2.9	1.1		0.1	0.2		0.0	0.0		0.1	0.2
Vesicle fill - opaque					1.1	0.7		2.0	0.9		0.8	0.6		0.3	0.3
Vesicle fill - clear					1.0	0.6		0.0	0.0		0.0	0.0		0.7	0.5
	B17-362	RF		B17-168	RF		B17-357	RF		B17-359	RF		B17-376	RF	
	solid rock %	whole rock %	2σ	solid rock %	whole rock %	2σ	solid rock %	whole rock %	2σ	solid rock %	whole rock %	2σ	solid rock %	whole rock %	2σ
Vesicles		55.3	3.1		29.7	2.9		82.8	2.4		56.7	3.1		35.3	3.0
Groundmass	86.4	36.2	3.3	92.0	64.0	2.1	90.3	14.0	4.7	87.1	36.4	3.3	86.6	52.8	2.8
Plagioclase - U	0.0	0.0	0.0	0.0	0.0	0.0	0.0	0.0	0.0	0.0	0.0	0.0	0.0	0.0	0.0
Olivine - U	9.8	4.1	2.9	7.2	5.0	2.0	8.4	1.3	4.5	4.1	1.7	1.9	2.1	1.3	1.2
Olivine - PA	0.0	0.0	0.0	0.6	0.4	0.6	0.0	0.0	0.0	0.0	0.0	0.0	8.9	5.4	2.3
Olivine - CA	0.0	0.0	0.0	0.0	0.0	0.0	0.0	0.0	0.0	0.0	0.0	0.0	1.0	0.6	0.8
Pyroxene - U	3.8	1.6	1.9	0.3	0.2	0.4	1.3	0.2	1.8	8.9	3.7	2.8	0.0	0.0	0.0
Pyroxene - PA	0.0	0.0	0.0	0.0	0.0	0.0	0.0	0.0	0.0	0.0	0.0	0.0	1.5	0.9	1.0
Pyroxene - CA	0.0	0.0	0.0	0.0	0.0	0.0	0.0	0.0	0.0	0.0	0.0	0.0	0.0	0.0	0.0
Vesicle fill - yellow		2.7	1.0		0.6	0.5		1.6	0.8		0.7	0.5		0.0	0.0
Vesicle fill - opaque		0.1	0.2		0.1	0.2		0.1	0.2		0.8	0.6		3.6	1.2
Vesicle fill - clear		0.0	0.0		0.0	0.0		0.0	0.0		0.0	0.0		0.1	0.2

3.4.2.2 Major Element Oxides

Whole rock XRF indicates that the basalts of KI have minor amounts of enrichment in MgO (~2x), Fe_2O_3 (~1.3x), and SiO_2 (~1.3x) (enrichment values based on re-normalization; Figure 10 & Table 7). The slight enrichments of MgO and SiO_2 are a result of layered amorphous Si-Mg-Al precipitates within vesicles (Figure 11). Fe_2O_3 enrichment is the result of ~20 μm dendritic iron precipitates in fractures that appear to be magnetite based on the equant shape seen in SEM/EDS imagery and lack of Ti that was seen in the KK precipitates (Figure 12). Although the Harker diagrams show an apparent depletion of SiO_2 relative to the unaltered sample, SiO_2 must have been added to the sample in order to achieve that little decrease in the normalized rock when balanced against the relative increases in MgO and Fe_2O_3. The enrichment of SiO_2 is due to silica precipitates within vesicles observable in hand sample and microscopy.

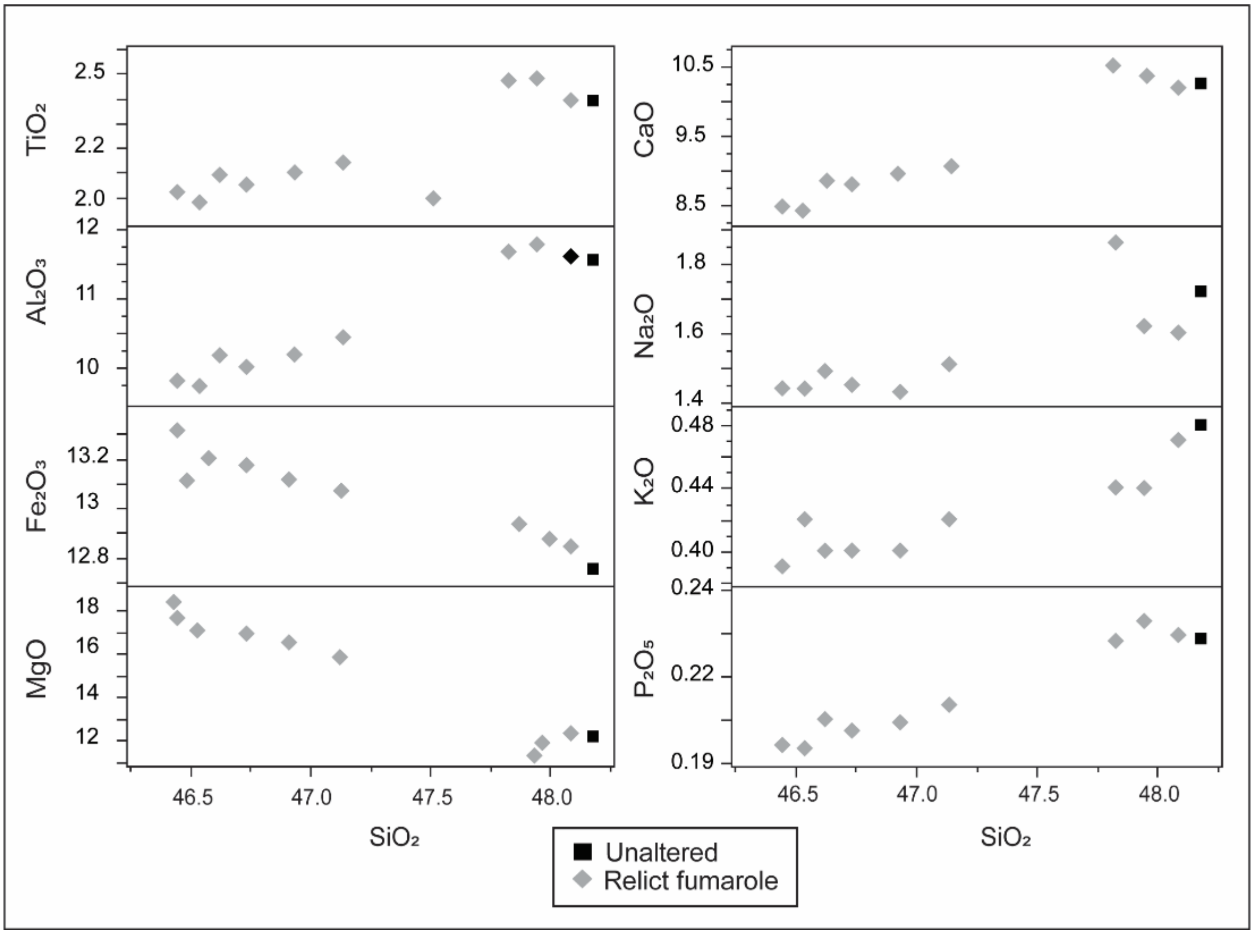

Figure 10: Major element oxide Harker diagram for relict fumaroles of Kilauea Iki. Note the increase in Fe_2O_3 and MgO as compared to the unaltered sample. Fe_2O_3 increases from 12.8 to 13.3 wt%, and MgO increases from 12 to 18 wt%.

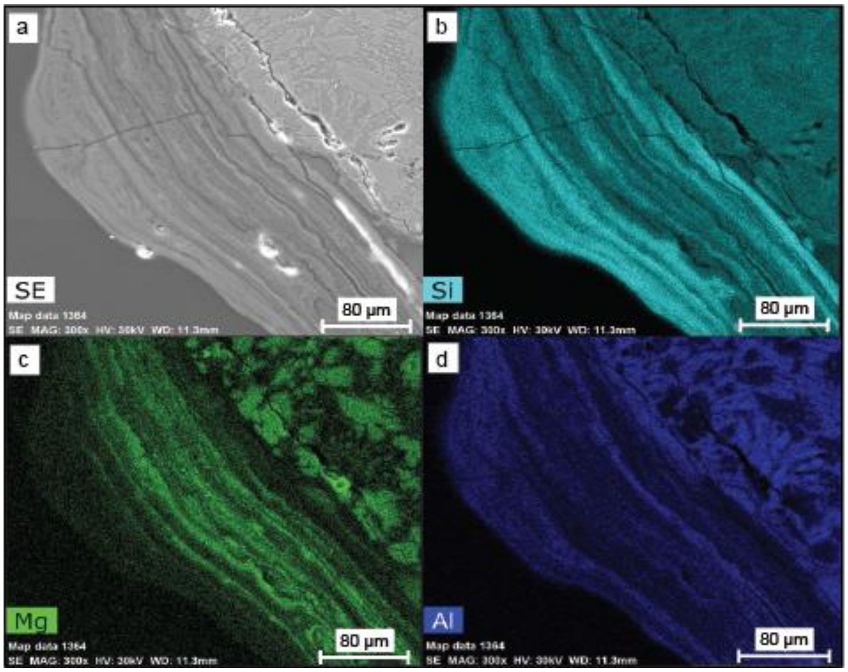

Figure 11: SEM/EDS imagery showing amorphous silica precipitate layered with amorphous Al and Mg in a high-density relict fumarole of Kilauea Iki (152). a) Secondary electron (SE) image of vesicle fill; b) Energy Dispersive Spectroscopy (EDS) element map showing Si; c) EDS element map showing Mg; d) EDS element map showing Al.

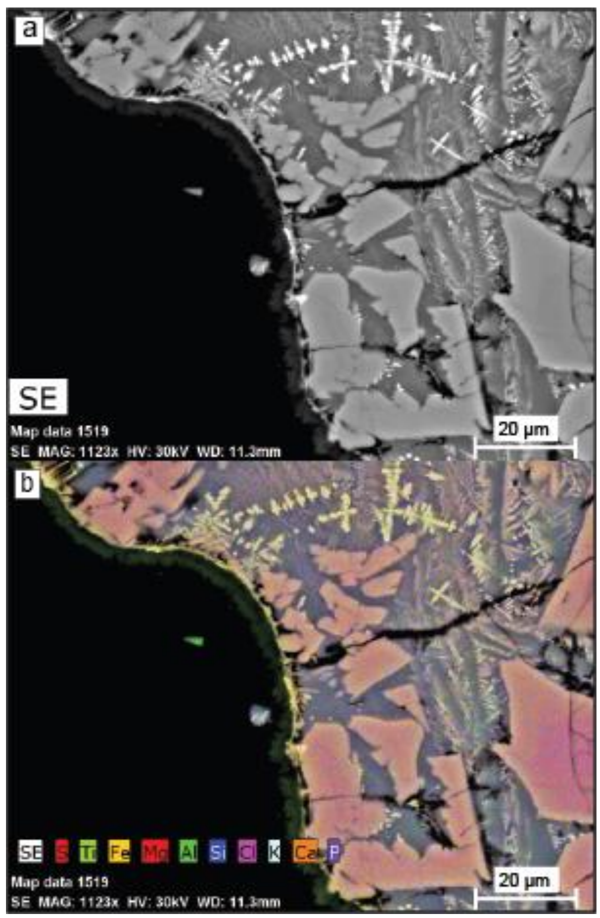

Figure 12: SEM/EDS imagery showing dendritic precipitates within fractures of high-density relict fumarole (152) of Kilauea Iki. a) SE image showing dendritic patterns within small rock fractures; b) EDS map showing the accumulation of Fe in the dendrites. Equant structure indicates the precipitate is magnetite.

Table 7: XRF major element oxide data from meteoric fumaroles associated with Kilauea Iki reported as wt. %. Normalized to 100% Volatile-free with all Fe as Fe_2O_3.

Samples	Alteration	SiO_2	TiO_2	Al_2O_3	Fe_2O_3	MnO	MgO	CaO	Na_2O	K_2O	P_2O_5	Total	LOI
114	U	48.18	2.39	11.57	12.76	0.17	12.24	10.26	1.72	0.48	0.23	100	0.59
152	RF-HD	47.94	2.48	11.79	12.89	0.17	12.04	10.39	1.62	0.44	0.24	100	-0.25
338	RF-HD	46.93	2.10	10.20	13.11	0.17	16.48	8.97	1.43	0.40	0.20	100	-0.63
362	RF-HD	47.14	2.14	10.45	13.07	0.17	15.83	9.06	1.51	0.42	0.21	100	-0.51
168	RF-LD	47.82	2.47	11.68	12.95	0.17	11.85	10.51	1.86	0.44	0.23	100	-0.69
339	RF-LD	46.62	2.09	10.19	13.19	0.17	16.81	8.83	1.49	0.40	0.21	100	-0.52
357	RF-LD	46.54	1.98	9.74	13.11	0.17	17.94	8.46	1.44	0.42	0.20	100	-0.69
295	RF	48.08	2.40	11.62	12.85	0.17	12.38	10.20	1.60	0.47	0.23	100	-0.51
359	RF	46.44	2.02	9.82	13.32	0.17	17.71	8.49	1.44	0.39	0.20	100	-0.42
376	RF	46.73	2.05	10.02	13.18	0.17	16.98	8.81	1.45	0.40	0.20	100	-0.52

3.4.2.3 Trace Elements

Trace elements associated with KI fumaroles vary little from the unaltered sample, with the exception of sulfur, which is enriched in two samples (338 & 362) that have higher densities (44% vesicularity compared to an average of 52%). We infer that this enrichment is a result of original sulfuric gases and subsequent precipitates preserved in poorly connected interior vesicles since emplacement. The lower vesicularity of these samples could have resulted in lower permeability and, therefore, increased protected from hydrothermal or meteoric dissolution. The remainder of the samples are sulfur-depleted (Figure 13 & Table 8).

Table 8: XRF trace element analyses from meteoric fumaroles associated with Kilauea Iki reported in ppm.

Sample	**114**	**152**	**338**	**362**	**168**	**339**	**357**	**295**	**359**	**376**
Alteration	**U**	**RF-HD**	**RF-HD**	**RF-HD**	**RF-LD**	**RF-LD**	**RF-LD**	**RF**	**RF**	**RF**
Ba	99	97	98	81	108	93	86	87	65	79
Ce	35	30	30	24	35	30	27	29	18	18
Cr	1043	837	1552	1266	1161	1582	1776	912	1225	1211
Cu	96	100	95	88	109	88	89	104	80	91
Ga	18	18	16	15	19	16	15	16	13	15
La	9	14	10	10	12	12	10	10	10	8
Nb	16	17	14	13	17	14	13	15	12	14
Nd	29	18	32	27	29	38	37	19	19	22
Ni	412	382	695	613	414	733	826	401	683	695
Pb	1	2	1	1	2	2	2	1	0	1
Rb	9	10	8	8	10	8	7	10	8	8
Sc	28	28	26	24	30	27	26	26	21	24
Sm	5	4	5	4	5	5	5	4	4	4
Sr	322	318	286	265	341	283	269	287	226	257
Th	0	0	1	0	0	0	0	0	0	0
U	0	0	0	0	0	0	0	0	0	0
V	293	298	267	246	308	266	249	267	216	234
Y	20	23	18	17	21	18	17	21	17	18
Zn	98	98	102	95	108	106	104	92	85	92
Zr	146	145	133	125	156	136	128	131	107	117
Cl	83	62	75	66	83	80	81	59	102	59
F	334	249	273	330	238	284	197	291	318	218
S	532	62	7791	1393	545	379	291	92	0	132

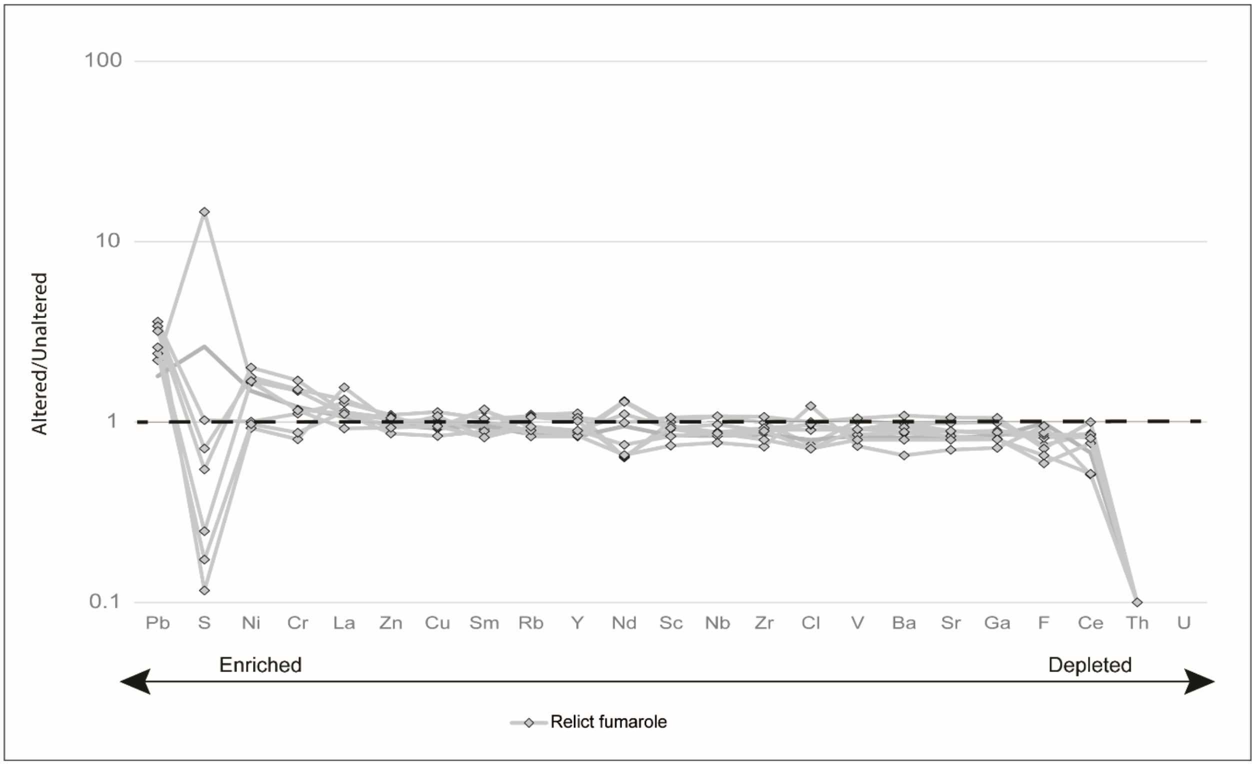

Figure 13: Spider diagram of Kilauea Iki trace element concentrations normalized to unaltered and sorted by mean enrichment (highest to lowest). Dashed line indicates unaltered sample. Sulfur exhibits the largest enrichment, followed by Pb and Cl. Values for Th was assigned small non-zero numbers (0.001) based on their mean non-normalized concentrations, due to the inability to normalize to 0 ppm.

3.4.3 Mauna Ulu: Meteoric Fumaroles & Syn-emplacement Alteration

3.4.3.1 Petrography

The basalts associated with active and relict meteoric fumaroles and syn-emplacement alteration at MU are dark gray to slightly reddish-orange to bright red, indicating a varying degrees of iron oxidation. Most of the samples have secondary ~ 0.2 – 1 mm silica growths within vesicles, and some have 2-5 mm of silica stalagmites growing on their surface. These stalagmites were cut off the surface during billet cutting in order to make thin sections of the interior of the rock. The unaltered sample consists of 90 ± 2 % groundmass, 2 ± 1% plagioclase, 6 ± 2% olivine, and 2 ±

1% pyroxene. The altered basalts are characterized by a mean of 83 ± 3% tachylite-rich groundmass, 6 ± 2% unaltered olivine, and 2 ± 1% unaltered clinopyroxene, normalized to solid rock. Partially altered phenocrysts of olivine and pyroxene in active and relict fumaroles account for a mean of 1 ± 1% and 0.5 ± 0.6% of the solid rock, respectively. Non-normalized counts show a mean vesicularity of 56 ± 3% with 5 ± 1% of the total vesicles containing amorphous, layered silica precipitates.

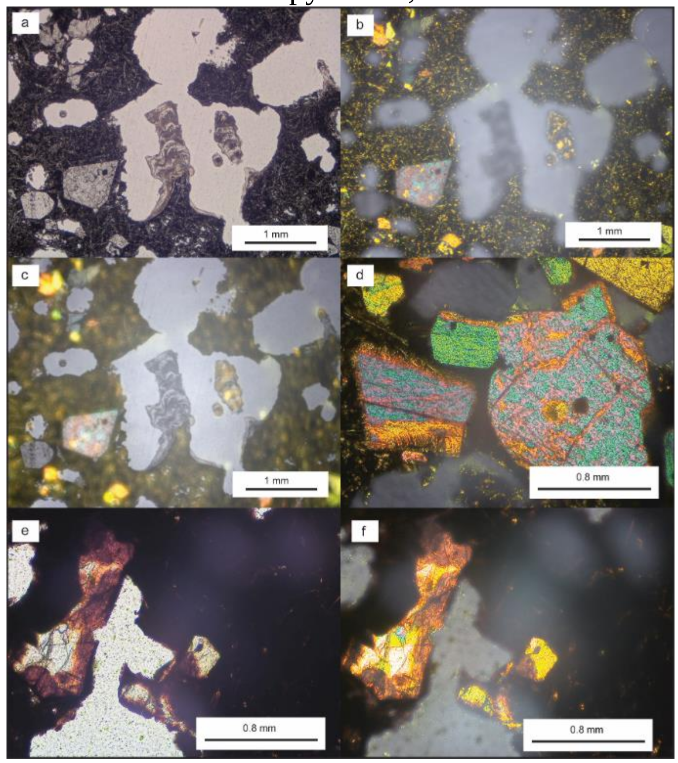

Figure 14: Photomicrographs showing the different types of alteration found at MU. a) PPL image of groundmass, phenocrysts, and vesicle precipitates in AF- 100079; b&c) AF-100079 in XP showing the vesicle precipitates and cryptocrystalline groundmass; d) XP image of AF-100079 showing the minor alteration to iddingsite on the rims of olivine phenocrysts; e) PPL image of RF-100040 showing extensive alteration to olivine phenocrysts; f) RF-100040 in XP.

The alteration within this system is on edges and in fractures of olivine and pyroxene phenocrysts and occurs as iddingsite (Figure 14). Layered silica precipitates are found within vesicles. Two active high-temperature fumarole samples (10068 & 100100) exhibit authigenic clay alteration (Table 9). High temperature active fumarole (100068) exhibits the highest degree of alteration to smectite and also has alteration to palagonite. This sample has 24 ± 3% clay alteration and 20 ± 2% palagonite alteration. This sample is unique from the others as it is composed of sideromelane, which accounts for 47 ± 4% of the solid rock, with 8 ± 2% olivine and 1 ± 1% pyroxene phenocrysts (Figure 15). This sample has more alteration to clay as glass is more susceptible to alteration due to its thermodynamic instability resulting from its weak internal structure and substantial space between molecules (Fisher and Schmincke, 1984). Interestingly, both of the samples with smectite alteration were collected from the rim of the ‘Ālo‘i crater on the west flank of MU. As a result, this area may have had more sustained hydrothermal activity as opposed to Kilauea Iki or elsewhere at MU and may have experienced syn-emplacement quenching with external water to create the sideromelane not seen elsewhere. These samples also contain the most vesicle precipitates, which have been found to grow more quickly in acidic systems (Chemtob and Rossman, 2014).It is possible that there was a brief period of magmatic hydrothermal activity at MU that caused the increased alteration in some areas, however, if it occurred it was not prolonged enough to have removed the clays and completely altered the rocks to opal as seen in the magmatic system at KK.

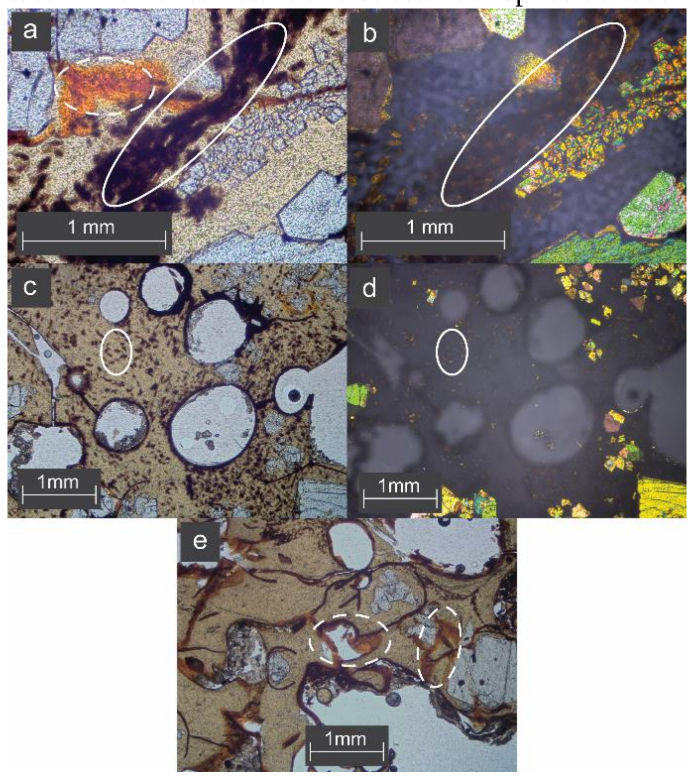

Figure 15: Photomicrograph of AF-100068 showing alteration to smectite (solid circle) and palagonite (dashed circle); a) PPL image of sideromelane glass with smectite and palagonite alteration; b) Image (a) in XPL; c) Beginning stages of smectite alteration within glass; d) Image (c) in XPL; e) PPL image of

Syn-emplacement altered rocks at MU have a mean of 92 ± 3% tachylite groundmass and 4 ± 2% olivine and pyroxene phenocrysts (8 ± 3% total phenocrysts). Alteration was minimal, with partially altered olivine accounting for 0.5 ± 0.7% of the solid rock. Alteration within the olivine occurs as iddingsite along rims and within fractures (**Error! Reference source not found.**).

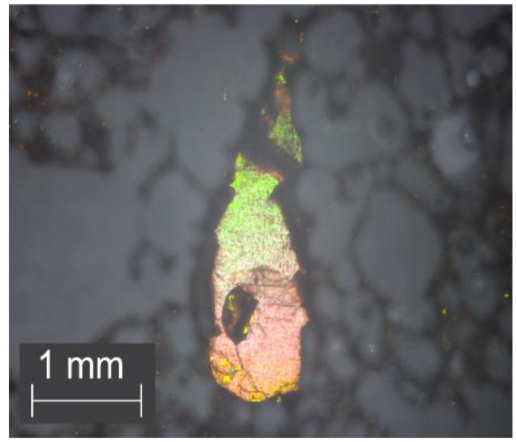

Figure 16: Partially altered olivine set in tachylite in a vesicle rich syn-emplacement altered rock (100611).

All of the samples with >50% vesicularity exhibit an increase in Al_2O_3, Fe_2O_3, and MgO. Sample 100068, the only sideromelane-rich sample in the suite, has 37% vesicularity but is consistent with the enrichment pattern for those with >50% vesicles. The enrichment pattern in this sample might be the result of sideromelane glass, which is less stable and more susceptible to alteration. This suggests that both glass-rich groundmass and increased surface area from higher vesiculation may contribute to larger changes within the rocks. While this makes sense conceptually, it should also be noted that there is not a strong correlation between these factors when viewed across the dataset as a whole; this lack of correlation could either indicate that the effects of sideromelane and porosity are not meaningful to the degree of alteration or that their contributions are small relative to the contributions alteration style and duration.

Table 9: Point count data from Mauna Ulu normalized to vesicle free (solid rock %), non-normalized (whole rock %) and standard deviation within 2σ. U = Unaltered; PA = Partially altered

	100108	U		100100	AF - HT (halo)		100093	AF - LT		100079	AF - HT	
	solid rock %	whole rock %	2σ	solid rock %	whole rock %	2σ	solid rock %	whole rock %	2σ	solid rock %	whole rock %	2σ
Vesicles		37.4	3.1		37.3	3.1		60.9	3.6		60.4	2.6
Groundmass	90.5	56.3	2.3	85.4	49.0	3.0	92.6	36.1	3.1	92.0	33.1	2.4
Plagioclase - U	1.8	1.1	1.1	0.0	0.0	0.0	0.0	0.0	0.0	0.0	0.0	0.0
Plagioclase - PA	0.0	0.0	0.0	0.0	0.0	0.0	0.0	0.0	0.0	0.0	0.0	0.0
Olivine - U	5.9	3.7	1.9	10.1	5.8	2.5	7.0	2.7	3.0	5.4	1.9	2.0
Olivine - PA	0.0	0.0	0.0	0.7	0.4	0.7	0.0	0.0	0.0	1.2	0.4	1.0
Pyroxene - U	1.8	1.1	1.1	1.7	1.0	1.1	0.4	0.1	0.7	0.8	0.3	0.8
Pyroxene - PA	0.0	0.0	0.0	0.2	0.1	0.3	0.0	0.0	0.0	0.6	0.2	0.7
Smectite	0.0	0.0	0.0	1.9	1.1	1.1	0.0	0.0	0.0	0.0	0.0	0.0
Palagonite												
Vesicle fill - yellow		0.3	0.3		1.0	0.6		0.0	0.0		0.9	0.5
Vesicle fill - opaque		0.1	0.2		3.7	1.2		0.1	0.3		0.0	0.0
Vesicle fill - clear		0.0	0.0		0.6	0.5		0.0	0.0		2.8	0.9

	100068	AF - HT		100040	RF		100130	RF		100052	SE	
	solid rock %	whole rock %	2σ	solid rock %	whole rock %	2σ	solid rock %	whole rock %	2σ	solid rock %	whole rock %	2σ
Vesicles		38.2	2.8		67.4	2.5		71.3	2.9		52.8	3.2
Groundmass	46.6	26.4	3.8	92.5	29.0	2.5	82.0	23.2	4.6	91.7	39.6	2.7
Plagioclase - U	0.0	0.0	0.0	0.0	0.0	0.0	0.0	0.0	0.0	0.0	0.0	0.0
Plagioclase - PA	0.0	0.0	0.0	0.0	0.0	0.0	0.0	0.0	0.0	0.0	0.0	0.0
Olivine - U	6.1	3.5	1.8	0.5	0.1	0.6	8.5	2.4	3.3	3.7	1.6	1.8
Olivine - PA	1.5	0.8	0.9	2.7	0.9	1.6	0.0	0.0	0.0	0.5	0.2	0.7
Pyroxene - U	1.2	0.7	0.8	0.0	0.0	0.0	2.8	0.8	2.0	4.2	1.8	1.9
Pyroxene - PA	0.1	0.1	0.3	1.1	0.4	1.0	0.0	0.0	0.0	0.0	0.0	0.0
Smectite	24.2	13.7	3.3	0.0	0.0	0.0	0.0	0.0	0.0	0.0	0.0	0.0
Palagonite	20.4	11.6	1.8	3.2		0.0	6.7	1.9	0.9			
Vesicle fill - yellow											3.5	1.2
Vesicle fill - opaque		0.0	0.0		0.0	0.0		0.0	0.0		0.5	0.4
Vesicle fill - clear		5.0	1.3		1.2	0.6		0.4	0.4		0.0	0.0

3.4.3.2 Major Element Oxides

Petrographic analysis and SEM/EDS imagery of active fumaroles reveals some alteration within phenocrysts, precipitates within vesicles, and smectite and palagonite alteration; however, unlike KK and KI, these precipitates are not layered with other elements (Figure 17). Figure 17b shows Si-Ca layering in the precipitation on the right; this was not seen in other MU precipitates. The alteration here is minor and has not resulted in any major enrichment or depletion in MEs. The minor enrichment is predominantly seen in the active fumaroles on the west flank of MU around the ʻĀloʻi crater, with SiO_2, TiO_2, Al_2O_3, Fe2O_3, and MgO, all ~1.1x greater than the unaltered samples based on renormalized concentrations (**Error! Reference source not found.**Figure 19Figure 19 & Table 10).

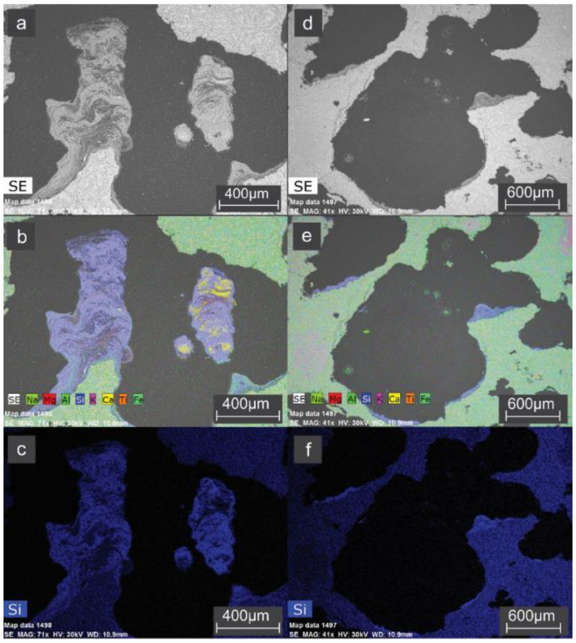

Figure 17: SEM/EDS map of AF-100100 from the west flank showing amorphous silica precipitates growing within vesicles. a)Secondary electron (SE) image of the area of interest; b) full element map showing the silica precipitation which lacks other elements; c) Si map showing concentrations of silica; d, e, & f) Same as a, b, & c, with a different and less filled vesicle shown.

Syn-emplacement altered rocks did not exhibit any noticeable enrichment or depletion patterns. Mean values for SiO_2 – Fe_2O_3 are slightly above the mean unaltered values, but within the standard deviation; mean values for MgO – K_2O_5 are slightly lower than the mean unaltered values, but again within the standard deviation (Table 10).

Table 10: Whole rock XRF for Mauna Ulu reported as wt. %. Normalized to 100% Volatile-free with all Fe as Fe_2O_3.

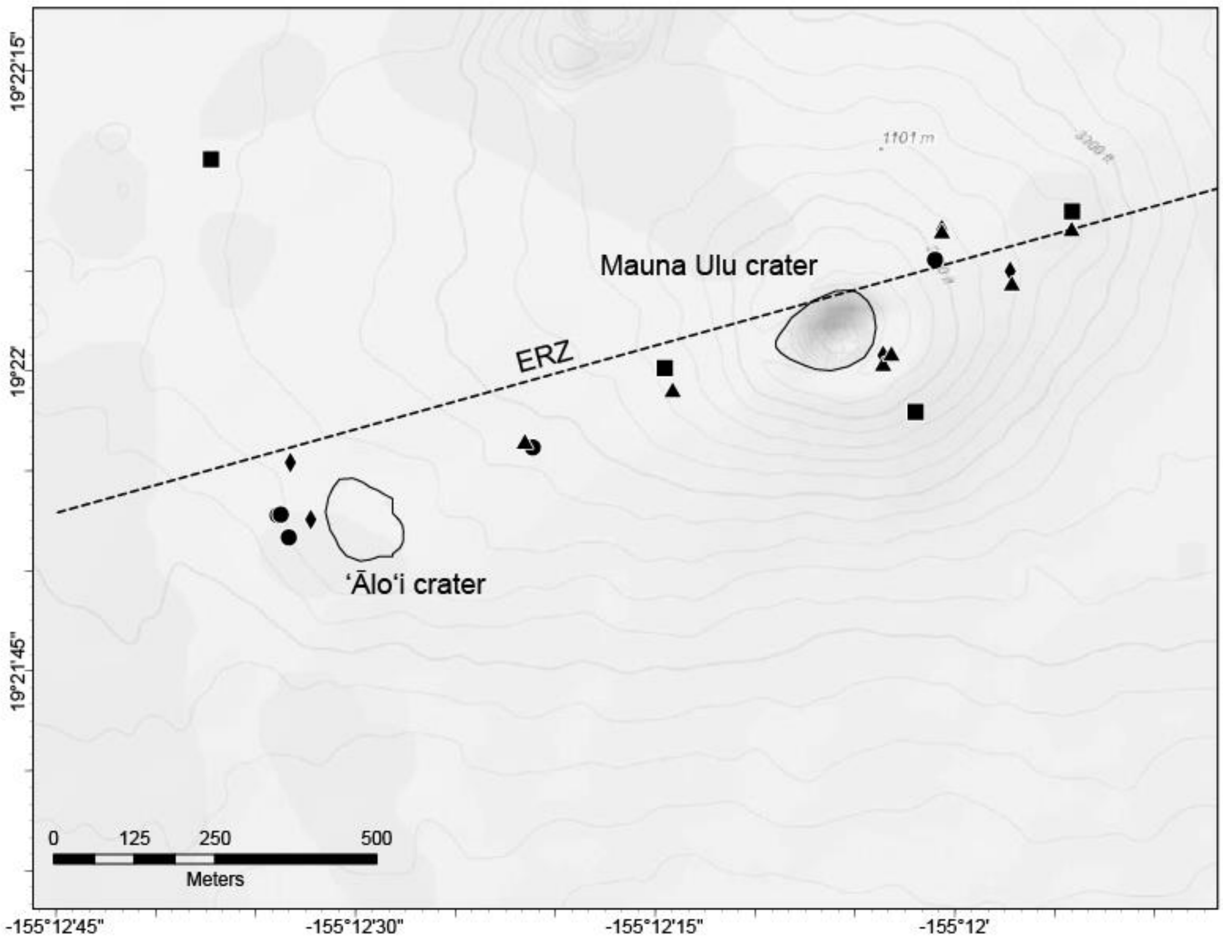

Figure 18: Map of Mauna Ulu showing sample locations on each of the flanks and the ʻĀloʻi and Maua Ulu craters. Basemap sources: Esri, HERE, Garmin, Intermap, increment P Corp., GEBCO, USS, FAO, NPS, NRCAN, GeoBase, IGN, Kadaster NL, Ordnance Survey, Esri Japan, METI, Esri China (Hong Kong), © OpenStreetMap contributors, and the GIS User Community.

3.4.3.3 Trace Elements

The trace element concentrations of MU rocks exhibit little change from the unaltered samples with the exception of sulfur, which is enriched in syn-emplacement and relict fumarole samples from the east and west flanks (Figure 20 & Table 11). None of the active meteoric fumarole samples exhibit sulfur enrichment. We infer that the sulfur enrichment is due to primary eruptive processes and post-emplacement weathering and hydrothermal processes have not removed sulfur-bearing minerals from the rocks. The relict fumarole enrichment of sulfur may be attributed to magmatic fumarole activity during and/or after the Mauna Ulu eruption. This activity may have ceased shortly after the eruption, and limited-to-no meteoric fumarolic activity has occurred since then. Given the lack of sulfur enrichment in active meteoric fumaroles at MU, we infer that meteoric fumarolic activity results in the depletion of native sulfur and sulfur-bearing minerals. Thus, the enrichments in sulfur observed in relict fumaroles suggest that these may have originally been short-duration magmatic fumaroles.

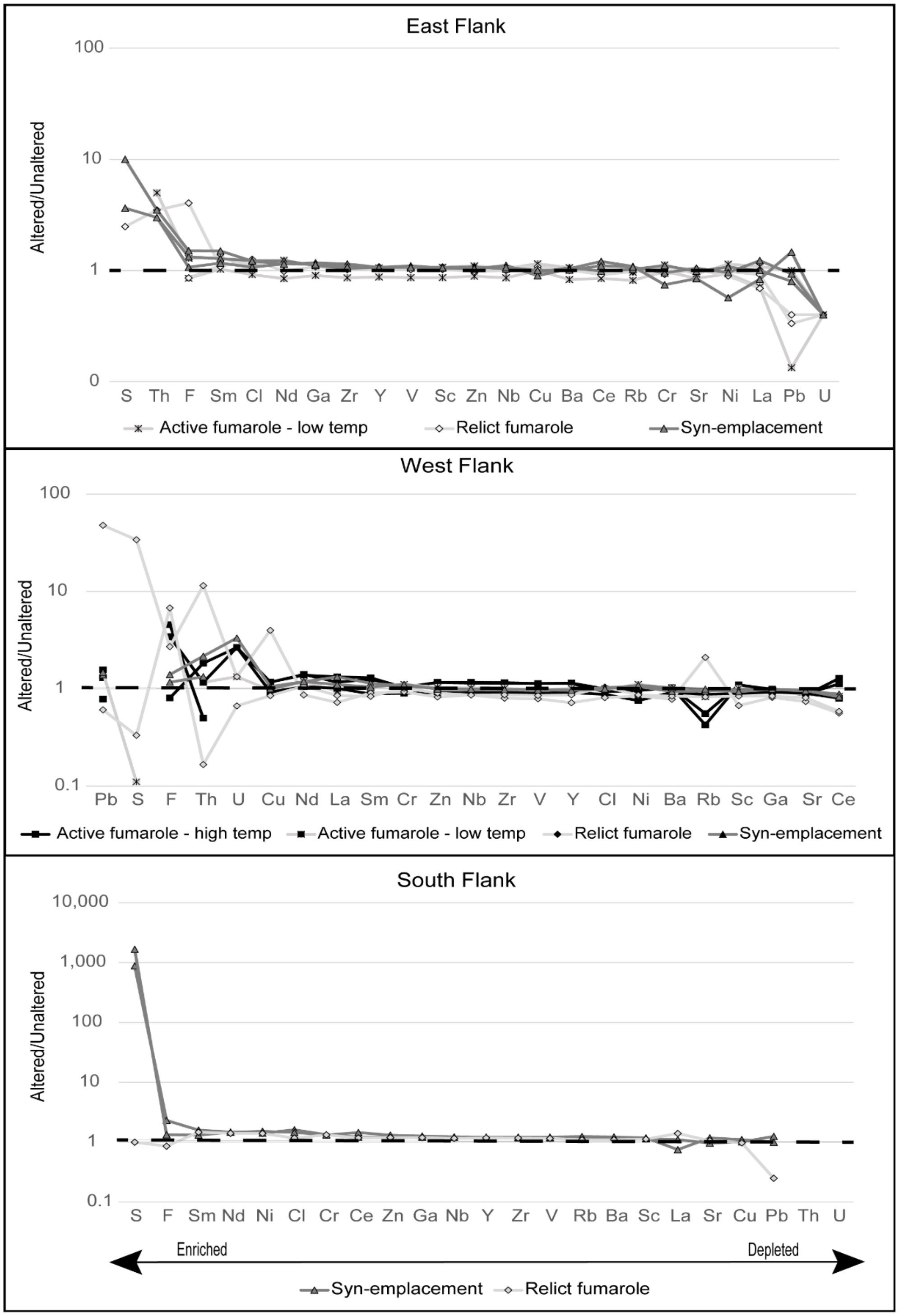

Figure 20: Spider diagram of Mauna Ulu trace element concentrations for the three flanks sampled, normalized to unaltered and sorted by mean enrichment (highest to lowest). Dashed line indicates unaltered sample.

Table 11: XRF trace element analyses from meteoric and syn-emplacement altered rocks associated with Mauna Ulu reported in ppm.

Sample	Alteration	U	Pb	Th	Sm	Rb	La	Y	Nd	Ce	Nb	Ga	Sc	Ba	Zn	Cu	Ni	Zr	Cl	F	Cr	V	Sr	S
100059	WF-U	0	2	1	4	8	6	23	17	22	12	17	31	73	102	102	366	128	91	91	896	282	280	99
53	WF-U	0	0	--	4	9	9	24	16	26	13	18	32	85	103	110	324	135	89	167	798	290	298	0
100068	WF-AF	0	1	1	6	5	10	27	23	27	15	17	34	81	120	124	333	152	90	104	873	325	257	0
100079	WF-AF	--	2	0	5	4	9	27	23	31	15	17	34	81	119	124	332	150	84	589	884	325	249	0
100100	WF-AF	0	2	1	4	7	8	22	17	19	12	16	28	73	94	98	261	120	79	443	764	259	261	0
100093	WF-AF	0	2	1	5	7	7	24	20	20	13	17	32	80	106	103	385	133	88	--	947	277	252	11
100040	WF-RF	0	55	7	4	18	6	17	14	13	11	14	21	62	85	423	292	105	73	350	790	226	214	3367
100130	WF-RF	0	1	0	4	7	7	21	17	14	11	15	26	66	93	90	299	114	94	876	861	244	234	33
100070	WF-SE	1	2	1	5	8	10	23	19	21	13	17	31	74	104	112	363	130	93	181	913	283	274	0
100052	WF-SE	--	2	1	5	8	8	23	19	20	13	17	29	81	102	106	376	129	90	151	944	279	277	0
100108	EF-U	--	2	0	4	8	8	22	16	20	12	16	29	76	96	101	343	124	84	215	827	266	275	83
100126	EF-AF	--	0	--	4	7	6	19	14	17	11	14	25	63	85	100	320	107	77	183	811	229	234	0
100718	EF-AF	1	2	1	5	8	9	23	20	19	13	17	31	80	105	116	392	129	92	276	931	279	256	0
100607	EF-RF	0	1	1	4	8	6	23	16	19	12	17	30	76	94	104	306	126	106	870	765	272	282	206
100140	EF-RF	--	1	--	4	8	8	24	19	18	13	18	31	77	103	109	335	133	98	184	872	285	285	0
100061	EF-SE	0	1	1	5	8	8	24	20	20	13	17	31	80	103	97	368	130	103	286	918	285	271	302
100611	EF-SE	0	2	1	5	9	7	24	19	24	14	18	31	78	99	90	195	143	102	323	615	294	233	831
100117	EF-SE	0	1	1	4	9	10	24	19	22	13	18	31	76	100	101	328	134	90	230	787	285	289	0
100704	SF-U	--	1	--	3	7	7	20	13	16	11	14	27	67	86	100	268	109	75	269	709	240	242	2
100700	SF-RF	--	0	--	5	8	10	23	19	19	12	17	30	73	102	98	375	128	88	230	937	277	256	2
100729	SF-SE	--	2	--	5	8	8	23	20	19	13	17	30	79	104	101	380	129	121	620	946	282	233	1758
100736	SF-SE	--	1	--	4	9	5	24	20	23	13	18	32	81	113	110	406	132	109	358	932	292	285	3324

3.5 Discussion

3.5.1 Alteration

The persistent addition of magmatic volatiles to the KK fumaroles near the active lava lake increased the water acidity, resulting in a much different style of alteration than seen in the meteoric fumaroles of KI and MU. The rocks from KK demonstrated the highest degree of alteration in both active and relict fumaroles. The depletion of major element oxides at KK is likely the result of increased solubility under acidic conditions allowing hydrothermal waters to carry more elements to the surface where they are incorporated into the overlying clays.

Basalts from the relict meteoric fumaroles of Kilauea Iki are relatively unaltered and changes to bulk chemistry appear to be largely driven by precipitation within fractures and vesicles. Groundwater of Kilauea is Mg-rich and contains anywhere from ~15 – 300 ppm of Mg, which is derived from both airborne salts from seawater and dissolution of Mg from subsurface rocks (Cox and Thomas, 1979); the Mg found in the water precipitates from solution into vesicles or forms smectite clays (Cox and Thomas, 1979). The basalts at KI contain a higher MgO wt. % than the other two flows in this study. Given the dearth of clays at KI, we infer that the MgO enrichment here is a result of the amorphous vesicle fill observed in the SEM/EDS element maps. We infer that these fumaroles did not have persistent magmatic activity after the initial emplacement; rather, the red coloration in KI basalts appears to be the result of continual low-temperature meteoric hydrothermal circulation and atmospheric oxygen exposure.

While the major element enrichment/depletions patterns in all sample types from Mauna Ulu are smaller than those at KI, the MU samples exhibit greater physical alteration with regard to palagonite, iddingsite, clays, and vesicle precipitates. Most of the alteration was associated with the west flank active fumaroles located on the edge of the ‘Ālo‘i pit crater. This region may have had magmatic fumarolic activity after the MU eruption due to its lower elevation on the ERZ, as compared to the near-summit area of MU, and previous eruption in this location. In addition, there was more persistent heat at MU than at KI, likely due to its location on the ERZ, which was experiencing long-term activity at Pu’u ‘O’o during the time of sample collection and was followed by the effusive eruptive sequence of 2018. Relict fumaroles and syn-emplacement altered samples from MU do not exhibit large changes in major or trace elements, with the exception of sulfur enrichment.

The CO_2- rich atmosphere of Mars could have caused more acidic hydrothermal systems than those on Earth. Understanding how CO_2-water-rock interaction influences the alteration of basalts allows us to better predict potential mineralogy in these systems on Earth and on Mars. Volatiles of Kilauea lavas are dominated by CO_2 (48.90 mole%), which contributes to the acidity of KK hydrothermal system (Symonds, 1998). Experimental studies indicate that basalt and CO_2-water-rock interactions result in secondary formation of ankerite and aluminosilicate minerals that precipitate into vesicles (Kanakiya et al., 2017). Rock dissolution dominates the release of cations into the water, facilitating the reactions necessary to precipitate secondary minerals from aqueous carbonic acid (Kanakiya et al., 2017). Although our study found layered amorphous silica precipitates rather than ankerite and aluminosilicates minerals, the processes of rock dissolution and secondary mineralization within pores as a result of CO_2-water-rock interactions appears to be similar. The removal of most major element oxides in the highly altered KK rocks and the secondary precipitation of opal into both the rock and the vesicles indicate that dissolution is a dominant process within the acidic KK hydrothermal system.

Interestingly, vesicularity did not play a role in alteration in any of the alteration styles studied. Increases in vesicularity leads a larger surface area of the rock that can be altered (Saar and Manga, 1999), however we didn't find a strong correlation between vesicularity and alteration in this study. Our organic geochemistry partners on the BASALT project measured total, isolated, and connected porosity of Mauna Ulu samples (Brady et al., *in review*). Using this data, we found no correlation between enrichment/depletion patterns of ME and TEs and total, isolated, and connected porosities of the samples.

All of the flows examined during this project are extremely young basalts ≤ 80 years old. Although this study does not account for temporal evolution of fumarolic activity, we can broadly resolve any major meteoric and/or magmatic fumarolic activity based on eruption dates. The KI lavas were the oldest but host the least developed fumarolic systems with regard to temperature or mineralization visible in the field at the time of the study. This is consistent with the opening of the tourist hiking trail across the KI lava lake less than 2 years after the eruption (Hawai'i Volcanoes National Park, personal communication, 2020), indicating a relatively quick return to safe conditions. Further, KI is located more off-axis from the ERZ than MU and further from the Halema'uma'u crater than KK, decreasing the strength of expected geothermal gradients located in the shallow subsurface there. While KK and MU samples were taken from lavas of similar ages, the former was perched near a persistent lava lake while the latter was located along the rift that fed the long-term Pu'u O'o eruptions and high-flux 2018 eruption. Based on this, it is likely that the KK fumaroles have been consistently magmatic over their existence experiencing cyclicity in the geochemistry of the hydrothermal waters, as evidenced by the SiO_2/Al_2O_3 layering within the precipitates. While the MU fumaroles may have experienced alternating periods of magmatic and meteoric activity based on the presence of sulfur enrichment in relict fumaroles, increased clay alteration, and layered silica precipitates, the lack of well-developed precipitate mounds at MU suggests that magmatic periods there are likely to have been brief.

3.5.2 Life and Mars

Our microbiology and organic geochemistry partners on the BASALT project have, to date, only examined the microbial communities from Mauna Ulu.

Relict fumaroles of MU hosted the largest mean biomass, followed by high temperature active fumaroles, syn-emplacement, and unaltered basalts and that low temperature active fumaroles and 1-2 m halos around the central vent of active meteoric fumaroles hosted the least biomass (Cockell et al., 2019). Phospholipid fatty acid (PLFA) biomarkers were used as an additional proxy measure for life at Mauna Ulu: PLFA was most abundant in syn-emplacement and unaltered samples, while high temperature fumaroles contained the least amount of PLFA (Brady et al., *in review*). Active fumaroles were found to host thermophiles, however, none of the organisms found in any of the different alteration styles were extremophiles, nor sulfur or iron-oxidizing (Cockell et al., 2019). Both Brady et al. (*in review*) and Cockell et al. (2019) indicate that halos (1 – 2 m) around all active fumaroles were the least habitable. The active fumarole samples that Cockell et al. (2019) and Brady et al. (*in review*) analyzed all have ME and TE compositions that are similar to the unaltered rocks, which indicates that a non-geochemical or mineralogical factor such as temperature fluctuation is causing the decreased habitability in active fumarole systems. Trace element concentrations of syn-emplacement samples are generally enriched in sulfur compared to unaltered samples, however enrichment/depletion patterns do not correlate with biomass or PLFA amounts. The decrease in biomass and PLFA in the halos around active fumaroles indicates that while habitability may change on sub-meter scales, the geochemistry of the rocks is not the driving force of change at MU.

Further, Cockell et al. (2019) conclude that although there are some extremophile communities living within the MU rocks, they are inconsistent with the communities one would expect to find on Mars as they do not utilize inorganic compounds within the rock for energy, relying instead on nutrients found in windblown loess and CO_2. The Cockell et al. (2019) metabolic findings are entirely consistent with the results reported here, in which we do not detect any measurable correlation between inhabitation (population density or diversity) and any mineralogical or geochemical measures of the host rock. We speculate, however, that this may be the result of an important factor: the thermal and chemical conditions in the MU samples were so similar to the surrounding rock that it failed to foster microbial communities that were measurably different from those typical of the larger region, thereby failing to create a filter for the desired endolithic extremophiles consistent with hypothesized martian communities. We anticipate that microbial analyses of the KK samples, which contained much larger changes in temperature, mineralogy, and geochemistry relative to the unaltered basalt, may provide much greater insight into the extremophile communities potentially compatible with hypothesized martian life. As such, we recommend that the BASALT team prioritize evaluation of KK samples, even at the expense of neglecting the KI samples, which showed the least mineralogical and geochemical alteration of the study areas.

The lack of extremophile and chemolithotroph communities at MU make this location a poor analog site for continued exobiology study. Hypotheses for life on Mars assume that microbes would need to be able to adapt to extreme environments and be able to survive on limited nutrients and energy sources (Horneck, 2000; Davila and Schulze-Makuch, 2016; Djokic et al., 2017), none of which appear well represented at MU. Further research into the habitability of magmatic fumaroles such as those found on the Kilauea caldera floor (KK) will improve our understanding of the distribution of endolithic microbial life on Kilauea, and how habitability changes across a variety of alteration styles on the volcano. The enrichment of SiO_2 at KK is indicative of prolonged acidic hydrothermal activity as well as the enrichment of S, Cl, and F (Chemtob and Rossman, 2014) and appears mineralogically more consistent with Home Plate on Mars (Squyres et al., 2008). The magmatic fumaroles at KK may also be more likely than the meteoric fumaroles at MU to host extremophile communities that are iron and sulfur-oxidizing, which may be closer to what could have existed on Mars when it was still wet and volcanically active during the Noachian - Hesperian. The enrichment of silica in the form of amorphous opal found on the Kilauea caldera floor also has the potential to preserve life and this aspect of opal enrichment in fumarolic systems should be studied as well (Jones and Renaut, 2007).

This research implies that future missions to Mars should be conducted in areas exhibiting magmatic fumarolic activity and containing S, F, P, Fe, Ti, and Cl-bearing minerals as well as amorphous opal, though upcoming microbiology and organic geochemistry results will indicate the extent to which these features are habitable by endolithic communities and how sensitive they are to changes across such a system.

Our research indicates that temperature and duration of magmatic hydrothermal activity plays an important role in the extent of alteration. Some of our low temperature and relict fumarole samples from KK exhibit enrichment/depletion patterns that match those of the high temperature fumarole altered basalts, indicating that these fumaroles may have once been high temperature and persisted for a longer time than those of the less altered samples. Further work should examine the temporal effects of hydrothermal alteration and how mineralogical and elemental changes occur throughout the lifecycle of a fumarole, including temperature and pH changes and how these changes impact microbial habitability. This should also include changes that occur after a fumarole has become relict. This information would improve our understanding the chemistry of the rocks through a fumarolic cycle and how endolithic microbial communities respond to these changes over time. By understanding the geochemistry of basalts in hydrothermal systems that exhibit evidence of extremophile endolithic microbial communities will allow us to prioritize targets on Mars.

3.6 Conclusions

We examined alteration of Kilauea basalts across various alteration styles to understand how water-rock interaction affects chemical and mineralogical changes in a rock. The alteration styles studied included syn-emplacement, relict fumaroles, and active fumaroles. Active fumarole alteration was further divided in magmatic, meteoric, and high and low temperature. These were compared to an unaltered sample collected from each location. We sampled three flows: Mana Ulu for syn-emplacement alteration, relict fumaroles, and active meteoric fumaroles; Kilauea Iki for relict meteoric fumaroles; and Kilauea caldera floor for active and relict magmatic fumaroles.

The highest degree of alteration was found in the magmatic fumaroles located on the Kilauea caldera floor, which exhibited ~20 times enrichment in both SiO_2 and TiO_2, and S concentrated to >1 wt. % of the rock. The most highly altered samples of this area are up to 93 wt. % SiO_2 in the form of amorphous opal. Original mineralogy within these rocks has been completely replaced with opal. SEM/EDS analyses displayed 10-20 μm anatase crystals and 70 μm dendritic titanomagnetite precipitates. Layered Si-Al precipitates were found in vesicles.

Relict meteoric fumaroles of Kilauea Iki exhibited minor enrichment in SiO_2, Al_2O_3, and Fe_2O_3, and ~2 times enrichment in MgO. The Si, Al, and Mg enrichment are a result of layered Si/Al/Mg precipitates, containing more Mg than Si. The Fe-enrichment is a result of ~20 μm dendritic magnetite precipitates within fractures near vesicles.

The meteoric fumarole system of Mauna Ulu exhibited little change in major and trace elements among any of the alteration styles present. While Cockell et al. (2019) and Brady et al. (*in review*) found that relict, unaltered, and syn-emplacement fumaroles contained the highest amounts of biomass and PLFA, there was no correlation between habitability metrics and any major or trace elements. This is likely due to the non-extremophile conditions in the MU samples, resulting in microbial communities that were not reliant on, and therefore not impacted by, changes in the basalt substrate.

Research on the habitability of the KK magmatic fumaroles is needed to better guide our understanding of endolithic microbial communities in extreme environments. These results may provide guidance to NASA when planning future robotic and manned Mars missions. With the data we currently have, we expect that regions on Mars that would make good targets would be areas that exhibit evidence of magmatic fumarolic activity and contain amorphous opal, which has the ability to preserve evidence of life.

Chapter 4: Discussion & Conclusions
4.1 Kilauea Calder Floor: Magmatic Fumaroles

The addition of magmatic gases to the groundwater sourcing the Kilauea caldera floor near the Halema'uma'u crater has resulted in a more acidic fumarole system consisting of CO_2, SO_2, H_2S, HCl, HF, and H_2, with a pH of ~1.5 (Goff and McMurtry, 2000). The hot acidic system of the Kilauea caldera floor allows for dissolution of major and trace elements in subsurface rocks which are transported and precipitated into near-surface and surface rocks. Native sulfur, clays, and silica precipitates were found as layered mounds above the rocks of the Kilauea caldera floor. In order to sample rocks in this location, we had to dig beneath these layers to find whole rock suitable for sampling. As a result of this, the rocks here exhibit the highest degree of alteration of all the alteration styles examined during this study. Hand samples of altered rocks range in color from light gray, reddish-orange, to a yellowish-white color (Figure 21).

Figure 21: Hand samples from the Kilauea caldera floor from left to right: Unaltered, high temperature active fumarole, low temperature active fumarole, relict fumarole showing a high degree of alteration corresponding with high temperature altered samples, relict fumarole showing a gradient of alteration from nearly-unaltered, to Fe-oxidized, with a small amount of opal on the bottom edge of the rock, a relict fumarole that is light gray with white opalized surface, and a relict fumarole that exhibits alteration similar to high temperature alteration.

Major element oxide analyses indicate that there is a 20x enrichment seen in both SiO_2 and TiO_2, which take the form of amorphous opal and anatase, respectively. Physically, the alteration in the magmatic fumarole samples consist of amorphous opal that has replaced the original mineralogy of the basalts, titanomagnetite dendrite precipitates in fractures within the rock near vesicles, and layered Si/Al precipitates within vesicles (Figure 22). These changes can be seen in hand sample, as well as petrographic and SEM imagery where the original phenocryst and microcryst forms are still visible but completely replaced with opal. Although clays were found at the surface, none of the rocks exhibited *in situ* clay alteration. We infer that clays formed here are the result of dissolution of the original rock material in the low pH water, which is then carried closer to the surface for precipitation.

Figure 22: Active fumarole sample from Mauna Ulu that exhibits beautiful silica precipitation in vesicles. All three study sites had rocks with similar silica precipitates that were destroyed during preparation. This sample's intact precipitates show, at a macroscopic level, what these look like.

4.2 Meteoric Fumaroles: Kilauea Iki

Kilauea Iki is relatively devoid of fumarolic activity, and all samples collected from this flow were from relict fumaroles. Alteration here was determined by the presence of minor amounts of steam with temperatures similar to the ambient air and by red discoloration of rocks from iron oxidation. The samples collected from the meteoric system of Kilauea Iki were minimally altered, with alteration predominantly consisting of precipitation within vesicles and some alteration of olivine and pyroxene rims to iddingsite. Hand samples are predominantly black/dark gray, with minor amounts of red coloration and white precipitates within vesicles (Figure 23).

Figure 23: Hand samples from Kilauea Iki from left to right: Unaltered, relict fumarole exhibiting no discoloration and white precipitates in vesicles, relict fumarole exhibiting some minor Fe-oxidation seen as red/orange coloration near vesicles, relict fumarole showing a higher degree of Fe-oxidation and white precipitates in vesicles.

Petrography showed minor amounts of alteration along edges and within fractures of olivine phenocrysts. Major element oxides had minor amounts of enrichment of SiO_2, Fe_2O_3, and a 2x increase in MgO. SEM/EDS analyses indicated that these enrichments are the result of layered Si/Mg precipitates within vesicles and dendritic magnetite precipitates in fractures within the rock near vesicles. The groundwater system beneath Kilauea is enriched in Mg which comes from both airborne salts derived from seawater and high temperature dissolution of Mg from rocks (Cox and Thomas, 1979). The lack of Cl and Na enrichment from seawater salts can be attributed to the minimal contribution of seawater as compared to rock dissolution and mobilization of elements that are found in higher concentrations within the basalt such as Mg. The Si/Mg saturated waters rise to the surface where Si and Mg precipitate out of solution. We infer that we see the Si/Mg precipitates in this system and not the others due to both the lack of heat here and the higher pH than magmatic fumaroles. Both of these factors can cause the Mg to stay in solution and be incorporated into the crystal lattice of clays. However, clays were not found in our samples, nor as mounds on the surface as seen on the Kilauea caldera floor.

4.3 Mauna Ulu: Syn-emplacement & Meteoric Fumaroles

Mauna Ulu exhibited the least amount of bulk chemical alteration of all the systems in this study, though they still contained noticeable mineralogical changes. The basalts of Mauna Ulu range in color from dark gray to bright red, indicating a varying amount of Fe-oxidation, and many samples contain visible silica precipitates (Figure 24). Some of the rocks exhibit alteration to clay and palagonite, as well as alteration of olivine rims and fractures to iddingsite. This is the only location that had clay and palagonite alteration of the rock. Although the Mauna Ulu samples exhibited more physical alteration of samples as compared to KI, this system exhibited the least change in major element oxides. In fact, none of the alteration styles exhibited any substantial ME enrichment/depletion as compared to unaltered samples. However, MU samples on all three flanks exhibit S and F enrichment greater than those of KI, indicating that this system has had more magmatic hydrothermal in its past than KI.

Figure 24: Hand samples from Mauna Ulu from left to right: Unaltered, high temperature active fumarole, relict fumarole, syn-emplacement altered rock.

Mauna Ulu lies along the ERZ, which is a source for higher, prolonged heat flux. The presence of smectite clay and palagonite alteration in some of the MU samples is inferred to be a result of the heat flux in this system, allowing for these alteration products to form more quickly than the intermittent, minimal and low temperature activity found on Kilauea Iki allows for.

4.4 Life and Mars

Our microbiology (Cockell et al., 2019) and organic geochemistry (Brady et al., *in prep*) partners on the BASALT project examined the microbial communities located on Mauna Ulu. They have not yet completed work on the other two flows.

Results from Cockell et al. (2019) indicate that relict fumaroles contain the largest mean biomass followed by high temperature active fumaroles, syn-emplacement altered, and unaltered basalts. Interestingly, this team found that low temperature fumaroles and 1-2 m halos around both high and low temperature fumaroles exhibited the least amount of biomass. This result is unexpected due to the occurrence of more water in these areas, and the halo around fumaroles is cooler than areas closer to the center of the fumarole, meaning it should be more habitable. Brady et al. (*in prep*) found the highest amounts of phospholipid-derived fatty acids (PLFA) in both syn-emplacement and unaltered rocks. Although these results differ slightly from Cockell et al. (2019), these alteration styles are similar in that they all have less consistent heat and water flow through them.

Cockell et al. (2019) identified thermophiles and acidophiles in some of the MU rocks. Thermophiles are microorganisms that live in high temperature between 41ºC and 121ºC, and acidophiles that can live in low pH conditions (≤ pH 2.0). Thermophile phyla found at MU were Deinococcus-Thermus and Firmicutes-Bacilli; the former were found in high and low temperature active fumaroles and in one replicate in a 1-2 m halo around an active fumarole, while the latter were found in low temperature active fumaroles and syn-emplacement samples. Acidobacteria, an acidophile, was found in every alteration style with abundances negatively correlated with *in situ* temperature. Although these extremophile communities exist on Mauna

Ulu, Cockell et al. (2019) determined that these communities are inconsistent with those expected for Mars. These communities, while living on the rock, are not utilizing inorganic compounds in the rock for energy; rather they are utilizing nutrients from dust and particulates that are blown in and settle on the rocks (Cockell et al., 2019)

Examination of biomass and PLFA with major element oxide and trace element data from this study found no correlation between abundances and enrichment/depletion patterns including for thermophile and acidophile species. We speculate that the reason we do not see a correlation between habitability and chemistry is a result of the similar chemistry found across all alteration styles that do not foster unique and diverse microbial communities, but rather these communities are representative of the larger region around Mauna Ulu.

The lack of extremophile and chemolithotroph (microbes that utilize inorganic compounds within rocks for energy) on Mauna Ulu make this a poor analog site for martian habitability. Previous research indicates that microbial life on Mars would need to be able to withstand extreme temperatures, radiation, high saline environments, dry environments, alkaline and acidic hydrothermal environments, etc. (Horneck, 2000; Davila and Schulze-Makuch, 2016; Djokic et al., 2017). While the microbes found at MU exist in a more extreme situation than normal terrestrial conditions, they don’t demonstrate the right adaptations to make them relevant. Further research by our partners on the BASALT project of the magmatic fumaroles located on the Kilauea caldera floor will improve our understanding of habitability across multiple different water-rock systems and potentially yield results that could be used to better guide future Mars missions.

We propose that NASA send future missions to areas on Mars that exhibit evidence of hydrothermal alteration as a result of magmatic fumaroles which will include amorphous opal, S, F, P, and Cl-bearing minerals indicative of magmatic activity. Spatially, we found no major ME & TE changes between more central fumarole rocks and those in 1 – 2 m halos (at MU only) around fumaroles; therefore orbital, robotic, or manned missions for locating potential hydrothermal regions only require resolution of 1 -2 m. Conversely, at μm – cm scale, physical alteration to clay, palagonite, iddingsite, and vesicle precipitates is present. The much smaller gradients in physical changes within the rock and in habitability require μm – cm resolution. As well as being an indicator of hydrothermal activity, amorphous opal has been found to preserve evidence of life and thus we want to make sure to target regions with amorphous opal for better potential to find preserved life (Jones and Renaut, 2007).

4.5 Letter to Future Students

This project was overwhelming, exciting, frightening, fun, engaging, and a learning experience. Getting a Master's degree is very challenging, as you have two years to try to fully engage with and understand new research, and two years is not a lot of time. Below I will discuss challenges and limitations of this project, what I would do to improve it with more time and money, and how this paper will potentially contribute to future NASA missions.

For my part, I came to this project late, which meant I was not present for any field work, making for a very sharp learning curve and many questions about the field deployments. Not being a part of discussions for choosing sample locations and not being present for the field deployments to witness and participate in the sample collection as a simulated Mars mission, meant filling in a lot of gaps using my advisor, and reading and rereading the papers that came out in 2019 as a part of the Astrobiology special issue on the BASALT project. This project involved travel to Hawai’i, limiting the number of times we could travel there for field work. Field work had to be conducted under simulated crewed Mars missions complete with communication lag time.

Other challenges centered on availability of equipment to analyze rocks. Idaho State University has some equipment which was useful to the project, but as with most research, much of the analyses needed to be performed at other schools, such as our XRF analyses. This means a potential delay in receiving data depending on the amount of work that school has ahead of you. The ISU XRD equipment failed before I could analyze my samples, and the replacement did not arrive until after I finished. The SEM/EDS was out of commission for an extended time due to a failing tip and construction in the building containing the equipment. Once the SEM was moved and set up, I was able to access it for more analyses before the COVID-19 pandemic shut everything down. These issues highlight the necessity of gathering data and analyzing it as early as possible in order to begin writing a thesis in a timely manner for a May graduation. Had I prioritized more data collection earlier in my thesis, XRD failure, SEM issues, and COVID-19 shutdowns would not have been as impactful for this project. These issues also highlight the need to adapt research to accessible and affordable tools. There are always more questions and more data that can be collected during the course of research and learning to prioritize questions and develop the research around time, equipment, and budget constraints will help keep research moving forward more smoothly. Along with the above, write early, write often. I found that writing my results section was where most of the understanding and confusion of my data came from. By writing about data early and often, you allow yourself more time to synthesize the results and gather further data that may be needed and relatively easy to collect, in my case this would have been more SEM/EDS analyses and point counts.

If I had unlimited time and resources for this project, I would have liked the ability to collect more samples, outside of a simulation, in order to get a more robust suite of samples that could potentially improve the significance of findings. I would have ideally liked a minimum of 5 samples from each sample location, collected from the center of the fumarole outward at 1 m intervals. The data collected from these samples could then be used to run ANOVA statistical analyses and create box plots. ANOVA analyses would allow for understanding small variation among groups of alteration styles and whether they are significant. Box Plots are useful for data visualization, and highlights differences between groups to see if the data overlaps or is completely different. I feel that enough samples to perform robust statistical analyses would give us better spatial resolution on changes within these systems and may have elucidated smaller scale variation not seen with the current number and distribution of samples. With more time and money, I would have also performed XRD analyses on my samples to determine what types of clays, if any, were in the rocks, and potentially find mineralogical changes not seen in petrographic and SEM/EDS work.

Another thing that time and money would help with is water research, which could possibly be a thesis project unto itself. Samples of water from each fumarole studied could have been analyzed for chemistry, acidity, microbial life, and more. Having a robust dataset of water chemistry could have really helped us understand these different systems and what in the water is causing the differences in chemistry seen in the rocks.

Finally, this paper potentially contributes to future spaceflight plans through a unique look at habitability across different styles of water-rock interactions, combining geochemistry, microbiology, and organic geochemistry. Through this unique lens, NASA can potentially use our data to target new regions of Mars that haven't been examined closely; or focus on currently known systems on Mars for a closer look. This research could then be expanded to other extraterrestrial volcanic bodies as more are discovered and help contribute to our overall understanding of our solar system and other planets in the universe that are similar to Earth.

References

Al-Hanbali, H.S., Sowerby, S.J., and Holm, N.G., 2001, Biogenicity of silici¢ed microbes from a hydrothermal system: relevance to the search for evidence of life on earth and other planets: Earth and Planetary Science Letters, p. 6.

Allen, C.C., Gooding, J.L., Jercinovic, M., and Keil, K., 1981, Altered basaltic glass: A terrestrial analog to the soil of Mars: Icarus, v. 45, p. 347–369, doi:10.1016/0019-1035(81)90040-3.

Atmosphere, U.S., 1976, US standard atmosphere: National Oceanic and Atmospheric Administration.

Baker, V.R., 2001, Water and the martian landscape: Nature, v. 412, p. 228–236, doi:10.1038/35084172.

Baker, I., and Haggerty, S.E., 1967, The alteration of olivine in basaltic and associated lavas: Contributions to Mineralogy and Petrology, v. 16, p. 257–273.

Bandfield, J.L., 2000, A Global View of Martian Surface Compositions from MGS-TES: Science, v. 287, p. 1626–1630, doi:10.1126/science.287.5458.1626.

Barnard, W.M., Halbig, J.B., and Fountain, J.C., 1990, Geochemical Study of Fumarolic Condensates from Kilauea Volcano, Hawaii: PACIFIC SCIENCE, v. 44, p. 10.

Beaton, K.H., Chappell, S.P., Abercromby, A.F.J., Miller, M.J., Kobs Nawotniak, S.E., Brady, A.L., Stevens, A.H., Payler, S.J., Hughes, S.S., and Lim, D.S.S., 2019a, Assessing the Acceptability of Science Operations Concepts and the Level of Mission Enhancement of Capabilities for Human Mars Exploration Extravehicular Activity: Astrobiology, v. 19, p. 321–346, doi:10.1089/ast.2018.1912.

Beaton, K.H., Chappell, S.P., Abercromby, A.F.J., Miller, M.J., Kobs Nawotniak, S.E., Brady, A.L., Stevens, A.H., Payler, S.J., Hughes, S.S., and Lim, D.S.S., 2019b, Using Science-Driven Analog Research to Investigate Extravehicular Activity Science Operations Concepts and Capabilities for Human Planetary Exploration: Astrobiology, v. 19, p. 300–320, doi:10.1089/ast.2018.1861.

Brady, A.L. et al., 2019, Strategic Planning Insights for Future Science-Driven Extravehicular Activity on Mars: Astrobiology, v. 19, p. 347–368, doi:10.1089/ast.2018.1850.

Brady, A.L., Gibbons, E., Sehlke A., Lim, D.S.S., Slater, G.F., in review, Microbial Community Distribution in Variously Altered Basalts: Insights into Astrobiology Sample Site Selection: Planetary and Space Science.

Bridges, J.C., and Warren, P.H., 2006, The SNC meteorites: basaltic igneous processes on Mars: Journal of the Geological Society, v. 163, p. 229–251, doi:10.1144/0016-764904-501.

Callac, N., Rommevaux-Jestin, C., Rouxel, O., Lesongeur, F., Liorzou, C., Bollinger, C., Ferrant, A., and Godfroy, A., 2013, Microbial colonization of basaltic glasses in hydrothermal organic-rich sediments at Guaymas Basin: Frontiers in Microbiology, v. 4, doi:10.3389/fmicb.2013.00250.

Chemtob, S.M., and Rossman, G.R., 2014, Timescales and mechanisms of formation of amorphous silica coatings on fresh basalts at Kīlauea Volcano, Hawai'i: Journal of Volcanology and Geothermal Research, v. 286, p. 41–54, doi:10.1016/j.jvolgeores.2014.08.029.

Clague, David A., and G. Brent Dalrymple. "The Hawaiian-Emperor volcanic chain. part I. Geologic evolution." Volcanism in Hawaii 1.1350 (1987): 5-54.

Cockell, C.S. et al., 2019, A Low-Diversity Microbiota Inhabits Extreme Terrestrial Basaltic Terrains and Their Fumaroles: Implications for the Exploration of Mars: Astrobiology, v. 19, p. 284–299, doi:10.1089/ast.2018.1870.

Cockell, C.S., 2014, Trajectories of Martian Habitability: Astrobiology, v. 14, p. 182–203, doi:10.1089/ast.2013.1106.

Cockell, C.S., Kelly, L.C., and Marteinsson, V., 2013, *Actinobacteria* —An Ancient Phylum Active in Volcanic Rock Weathering: Geomicrobiology Journal, v. 30, p. 706–720, doi:10.1080/01490451.2012.758196.

Costello, E.K., Halloy, S.R.P., Reed, S.C., Sowell, P., and Schmidt, S.K., 2009, Fumarole-Supported Islands of Biodiversity within a Hyperarid, High-Elevation Landscape on Socompa Volcano, Puna de Atacama, Andes: Applied and Environmental Microbiology, v. 75, p. 735–747, doi:10.1128/AEM.01469-08.

Cox, M.E., and Thomas, D.M., 1979, Assessment of Geothermal Resources in Hawaii: Number 3: Hawaii Institue of Geophysics.

Craddock, R.A., and Howard, A.D., 2002, The case for rainfall on a warm, wet early Mars: Journal of Geophysical Research: Planets, v. 107, p. 21-1-21–36, doi:10.1029/2001JE001505.

Damer, B., and Deamer, D., 2020, The Hot Spring Hypothesis for an Origin of Life: Astrobiology, v. 20, p. 429–452, doi:10.1089/ast.2019.2045.

Davila, A.F., and Schulze-Makuch, D., 2016, The Last Possible Outposts for Life on Mars: Astrobiology, v. 16, p. 159–168, doi:10.1089/ast.2015.1380.

Djokic, T., Van Kranendonk, M.J., Campbell, K.A., Walter, M.R., and Ward, C.R., 2017, Earliest signs of life on land preserved in ca. 3.5 Ga hot spring deposits: Nature Communications, v. 8, doi:10.1038/ncomms15263.

Duffield, W.A., Christiansen, R.L., Koyanagi, R.Y., and Peterson, D.W., 1982, Storage, migration, and eruption of magma at Kilauea volcano, Hawaii, 1971–1972: Journal of Volcanology and Geothermal Research, v. 13, p. 273–307, doi:10.1016/0377-0273(82)90054-3.

Dunfield, K.E., and King, G.M., 2004, Molecular Analysis of Carbon Monoxide-Oxidizing Bacteria Associated with Recent Hawaiian Volcanic Deposits: Applied and Environmental Microbiology, v. 70, p. 4242–4248, doi:10.1128/AEM.70.7.4242-4248.2004.

Edwards, C.S., Christensen, P.R., and Hamilton, V.E., 2008, Evidence for extensive olivine-rich basalt bedrock outcrops in Ganges and Eos chasmas, Mars: Journal of Geophysical Research, v. 113, doi:10.1029/2008JE003091.

Eggleton, R.A., Foudoulis, C., and Varkevisser, D., 1987, Weathering of Basalt: Changes in Rock Chemistry and Mineralogy: Clays and Clay Minerals, v. 35, p. 161–169, doi:10.1346/CCMN.1987.0350301.

Ehlmann, B.L., and Edwards, C.S., 2014, Mineralogy of the Martian Surface: Annual Review of Earth and Planetary Sciences, v. 42, p. 291–315, doi:10.1146/annurev-earth-060313-055024.

Fisher, R.V., and Schmincke, H.-U., 1984, Pyroclastic Rocks: Berlin, Heidelberg, Springer Berlin Heidelberg, doi:10.1007/978-3-642-74864-6.

Forget, F., 1997, Warming Early Mars with Carbon Dioxide Clouds That Scatter Infrared Radiation: Science, v. 278, p. 1273–1276, doi:10.1126/science.278.5341.1273.

Franz, H.B. et al., 2017, Initial SAM calibration gas experiments on Mars: Quadrupole mass spectrometer results and implications: Planetary and Space Science, v. 138, p. 44–54, doi:10.1016/j.pss.2017.01.014.

Garcia, M.O., Ito, E., Eiler, J.M., and Pietruszka, A.J., 1998, Crustal Contamination of Kilauea Volcano Magmas Revealed by Oxygen Isotope Analyses of Glass and Olivine from Puu Oo Eruption Lavas: v. 39, p. 15.

Garcia, M.O., Pietruszka, A.J., and Rhodes, J.M., 2003, A Petrologic Perspective of Kilauea Volcano’s Summit Magma Reservoir: Journal of Petrology, v. 44, p. 2313–2339, doi:10.1093/petrology/egg079.

Gislason, S.R., and Eugster, H.P., 1987, Meteoric water-basalt interactions. II: A field study in N.E. Iceland: Geochimica et Cosmochimica Acta, v. 51, p. 2841–2855, doi:10.1016/0016-7037(87)90162-1.

Gislason, S.R., Veblen, D.R., and Livi, K.J.T., 1993, Experimental meteoric water-basalt interactions: Characterization and interpretation of alteration products: Geochimica et Cosmochimica Acta, v. 57, p. 1459–1471, doi:10.1016/0016-7037(93)90006-I.

Glotch, T.D., and Bandfield, J.L., 2006, Determination and interpretation of surface and atmospheric Miniature Thermal Emission Spectrometer spectral end-members at the Meridiani Planum landing site: Journal of Geophysical Research, v. 11, doi:10.1029/2005JE002671.

Goff, F., and McMurtry, G.M., 2000, Tritium and stable isotopes of magmatic waters: Journal of Volcanology and Geothermal Research, v. 97, p. 347–396, doi:10.1016/S0377-0273(99)00177-8.

Golden, D.C., Ming, D.W., Morris, R.V., and Mertzman, S.A., 2005, Laboratory-simulated acid-sulfate weathering of basaltic materials: Implications for formation of sulfates at Meridiani Planum and Gusev crater, Mars: Journal of Geophysical Research, v. 110, doi:10.1029/2005JE002451.

Greeley, R., 1974, Geologic Guide to the Island of Hawaii: A Field Guide for Comparative planetary Geology: NASA CR 152416, 257 p.

Greeley, R., and Spudis, P.D., 1981, Volcanism on Mars: Reviews of Geophysics, v. 19, p. 13–41, doi:10.1029/RG019i001p00013.

Grotzinger, J.P. et al., 2014, A Habitable Fluvio-Lacustrine Environment at Yellowknife Bay, Gale Crater, Mars: Science, v. 343, p. 1242777–1242777, doi:10.1126/science.1242777.

Haberle, R.M., 1998, Early Mars Climate Models: Journal of Geophysical Research: Planets, v. 103, p. 28467–28479, doi:10.1029/98JE01396.

Hauber, E., Brož, P., Jagert, F., Jodłowski, P., and Platz, T., 2011, Very recent and wide-spread basaltic volcanism on Mars: RECENT WIDE-SPREAD VOLCANISM ON MARS: Geophysical Research Letters, v. 38, p. n/a-n/a, doi:10.1029/2011GL047310.

Heltz, R.T., Clague, D.A., Sisson, T.W., and Thornber, C.R., 2014, Petrologic Insights into Basaltic Volcanism at Historically Active Hawaiian Volcanoes: United States Geological Survey Professional Paper Professional Paper 1801.

Holcomb, Robin T. "Eruptive History and Long-Term Behavior of Kilauea Volcano" Volcanism in Hawaii 1.1350 (1987): 261-350.

Horneck, G., 2000, The microbial world and the case for Mars: Planetary and Space Science, v. 48, p. 1053–1063, doi:10.1016/S0032-0633(00)00079-9.

Hughes, S.S. et al., 2019, Basaltic Terrains in Idaho and Hawai‘i as Planetary Analogs for Mars Geology and Astrobiology: Astrobiology, v. 19, p. 260–283, doi:10.1089/ast.2018.1847.

Hurwitz, S., Goff, F., Janik, C.J., Evans, W.C., Counce, D.A., Sorey, M.L., and Ingebritsen, S.E., 2003, Mixing of magmatic volatiles with groundwater and interaction with basalt on the summit of Kilauea Volcano, Hawaii: Journal of Geophysical Research: Solid Earth, v. 108, doi:10.1029/2001JB001594.

Ingebritsen, S.E., and Scholl, M.A., 1993, The hydrogeology of Kilauea volcano: Geothermics, v. 22, p. 255–270, doi:10.1016/0375-6505(93)90003-6.

Jackson, M.G., Weis, D., and Huang, S., 2012, Major element variations in Hawaiian shield lavas: Source features and perspectives from global ocean island basalt (OIB) systematics: MAJOR ELEMENT VARIATIONS IN HAWAIIAN LAVAS: Geochemistry, Geophysics, Geosystems, v. 13, doi:10.1029/2012GC004268.

Jakosky, B.M., and Phillips, R.J., 2001, Mars' volatile and climate history: Nature, v. 412, p. 237–244, doi:10.1038/35084184.

Jones, B., and Renaut, R.W., 2007, Microstructural changes accompanying the opal-A to opal-CT transition: new evidence from the siliceous sinters of Geysir, Haukadalur, Iceland: Sedimentology, v. 54, p. 921–948, doi:10.1111/j.1365-3091.2007.00866.x.

Kanakiya, S., Adam, L., Esteban, L., Rowe, M.C., and Shane, P., 2017, Dissolution and secondary mineral precipitation in basalts due to reactions with carbonic acid: BASALT DISSOLUTION DUE TO CARBONIC ACID: Journal of Geophysical Research: Solid Earth, v. 122, p. 4312–4327, doi:10.1002/2017JB014019.

Kashefi, K., and Lovley, D.R., 2003, Extending the Upper Temperature Limit for Life: Science, New Series, v. 301, p. 934.

King, P.L., and McLennan, S.M., 2010, Sulfur on Mars: Elements, v. 6, p. 107–112, doi:10.2113/gselements.6.2.107.

Kobs Nawotniak, S.E. et al., 2019, Opportunities and Challenges of Promoting Scientific Dialog throughout Execution of Future Science-Driven Extravehicular Activity: Astrobiology, v. 19, p. 426–439, doi:10.1089/ast.2018.1901.

Konhauser, K.O., Schiffman, P., and Fisher, Q.J., 2002, Microbial mediation of authigenic clays during hydrothermal alteration of basaltic tephra, Kilauea Volcano: Geochemistry, Geophysics, Geosystems, v. 3, p. 1–13, doi:10.1029/2002GC000317.

Li, G. et al., 2016, Temperature dependence of basalt weathering: Earth and Planetary Science Letters, v. 443, p. 59–69, doi:10.1016/j.epsl.2016.03.015.

Lim, D.S.S. et al., 2019, The BASALT Research Program: Designing and Developing Mission Elements in Support of Human Scientific Exploration of Mars: Astrobiology, v. 19, p. 245–259, doi:10.1089/ast.2018.1869.

Marquez, J.J. et al., 2019, Future Needs for Science-Driven Geospatial and Temporal Extravehicular Activity Planning and Execution: Astrobiology, v. 19, p. 440–461, doi:10.1089/ast.2018.1838.

McMurtry, G.M., Fan, P., and Coplen, T.B., 1977, Chemical and Isotopic Investigations of Groundwater in Potential Geothermal Areas in Hawaii: American Journal of Science, v. 277, p. 438–458.

Miller, M.J., Miller, M.J., Santiago-Materese, D., Seibert, M.A., and Lim, D.S.S., 2019, A Flexible Telecommunication Architecture for Human Planetary Exploration Based on the BASALT Science-Driven Mars Analog: Astrobiology, v. 19, p. 478–496, doi:10.1089/ast.2018.1906.

Morris, R.V. et al., 2000, Mineralogy, composition, and alteration of Mars Pathfinder rocks and soils: Evidence from multispectral, elemental, and magnetic data on terrestrial analogue, SNC meteorite, and Pathfinder samples: Journal of Geophysical Research: Planets, v. 105, p. 1757–1817, doi:10.1029/1999JE001059.

Naughton, J.J., Greenberg, V.A., and Goguel, R., 1976, Incrustations and fumarolic condensates at kilauea volcano, Hawaii: field, drill-hole and laboratory observations: Journal of Volcanology and Geothermal Research, v. 1, p. 149–165, doi:10.1016/0377-0273(76)90004-4.

Neal, C.A., and Lockwood, J.P., 2003, Geologic Map of the Summit Region of Kilauea Volcano, Hawaii: United States Geological Survey I–2759, doi:10.3133/i2759.

Neukum, G., and Hiller, K., 1981, Martian ages: Journal of Geophysical Research: Solid Earth, v. 86, p. 3097–3121, doi:10.1029/JB086iB04p03097.

Payler, S.J., Mirmalek, Z., Hughes, S.S., Kobs Nawotniak, S.E., Brady, A.L., Stevens, A.H., Cockell, C.S., and Lim, D.S.S., 2019, Developing Intra-EVA Science Support Team Practices for a Human Mission to Mars: Astrobiology, v. 19, p. 387–400, doi:10.1089/ast.2018.1846.

Peck, D.L., Wright, T.L., and Moore, J.G., 1966, Crystallization of tholeiitic basalt in Alae Lava Lake, Hawaii: Bulletin Volcanologique, v. 29, p. 629–655, doi:10.1007/BF02597182.

Pollack, J.B., Kasting, J.F., Richardson, S.M., and Poliakoff, K., 1987, The case for a wet, warm climate on early Mars: Icarus, v. 71, p. 203–224, doi:10.1016/0019-1035(87)90147-3.

Richter, D.H., and Moore, J.G., 1966, Petrology of the Kilauea Iki Lava Lake, Hawaii: Professional Paper, doi:10.3133/pp537B.

Ruff, S.W. et al., 2011, Characteristics, distribution, origin, and significance of opaline silica observed by the Spirit rover in Gusev crater, Mars: Journal of Geophysical Research, v. 116, doi:10.1029/2010JE003767.

Ruff, S.W., Campbell, K.A., Van Kranendonk, M.J., Rice, M.S., and Farmer, J.D., 2020, The Case for Ancient Hot Springs in Gusev Crater, Mars: Astrobiology, v. 20, p. 475–499, doi:10.1089/ast.2019.2044.

Saar, M.O., and Manga, M., 1999, Permeability-porosity relationship in vesicular basalts: Geophysical Research Letters, v. 26, p. 111–114, doi:10.1029/1998GL900256.

Sehlke, A. et al., 2019, Requirements for Portable Instrument Suites during Human Scientific Exploration of Mars: Astrobiology, v. 19, p. 401–425, doi:10.1089/ast.2018.1841.

Seibert, M.A., Lim, D.S.S., Miller, M.J., Santiago-Materese, D., and Downs, M.T., 2019, Developing Future Deep-Space Telecommunication Architectures: A Historical Look at the Benefits of Analog Research on the Development of Solar System Internetworking for Future Human Spaceflight: Astrobiology, v. 19, p. 462–477, doi:10.1089/ast.2018.1915.

Sigurdsson, H., Houghton, B., Rymer, H., Stix, J., and McNutt, S., 1999, Encyclopedia of Volcanoes: Academic Press, 1417 p.

Skok, J.R., Mustard, J.F., Ehlmann, B.L., Milliken, R.E., and Murchie, S.L., 2010, Silica deposits in the Nili Patera caldera on the Syrtis Major volcanic complex on Mars: Nature Geoscience, v. 3, p. 838–841, doi:10.1038/ngeo990.

Squyres, S.W. et al., 2008, Detection of Silica-Rich Deposits on Mars: Science, v. 320, p. 1063–1067, doi:10.1126/science.1155429.

Stevens, A.H., Kobs Nawotniak, S.E., Garry, W.B., Payler, S.J., Brady, A.L., Miller, M.J., Beaton, K.H., Cockell, C.S., and Lim, D.S.S., 2019, Tactical Scientific Decision-Making during Crewed Astrobiology Mars Missions: Astrobiology, v. 19, p. 369–386, doi:10.1089/ast.2018.1837.

Stovail, W.K., 2009, GEOLOGY AND GEOPHYSICS MAY 2009:

Sun, V.Z., and Milliken, R.E., 2019, Characterizing the Mineral Assemblages of Hot Spring Environments and Applications to Mars Orbital Data: Astrobiology, doi:10.1089/ast.2018.2003.

Sun, S.-S., Nesbitt, R.W., and Sharaskin, A.Ya., 1979, Geochemical characteristics of mid-ocean ridge basalts: Earth and Planetary Science Letters, v. 44, p. 119–138, doi:10.1016/0012-821X(79)90013-X.

Swanson, D.A., Duffield, W.A., Jackson, D.B., and Peterson, D.W., 1979, Chronological narrative of the 1969-71 Mauna Ulu eruption of Kilauea Volcano, Hawaii: United States Geological Survey Professional Paper Professional Paper 1056, 55 p.

Symonds, R.B., 1998, Compositions, Origins, Emission Rates and Atmospheric Impacts of Volcanic Gases: U.S. Geological Survey 98–776, 12 p., https://pubs.usgs.gov/pp/1987/1350/pdf/chapters/pp1350_ch16.pdf (accessed May 2020).

Trainer, M.G. et al., 2019, Seasonal Variations in Atmospheric Composition as Measured in Gale Crater, Mars: Journal of Geophysical Research: Planets, v. 124, p. 3000–3024, doi:10.1029/2019JE006175.

Vago, J.L. et al., 2017, Habitability on Early Mars and the Search for Biosignatures with the ExoMars Rover: Astrobiology, v. 17, p. 471–510, doi:10.1089/ast.2016.1533.

Van Der Plas, L., and Tobi, A.C., 1965, A Chart for Judging the Reliability of Point Counting Results: American Journal of Science, v. 263, p. 87–90.

Vaniman, D.T. et al., 2014, Mineralogy of a Mudstone at Yellowknife Bay, Gale Crater, Mars: Science, v. 343, p. 1243480–1243480, doi:10.1126/science.1243480.

Varnes, E.S., Jakosky, B.M., and McCollom, T.M., 2003, Biological Potential of Martian Hydrothermal Systems: Astrobiology, v. 3, p. 407–414, doi:10.1089/153110703769016479.

Wilson, L., and Head, J.W., 1983, A comparison of volcanic eruption processes on Earth, Moon, Mars, Io and Venus: Nature, v. 302, p. 663–669, doi:10.1038/302663a0.

Wilson, L., and Head, J.W., 1981, Ascent and eruption of basaltic magma on the Earth and Moon: Journal of Geophysical Research: Solid Earth, v. 86, p. 2971–3001, doi:10.1029/JB086iB04p02971.

Wolfe, C.E.W., and Morris, J., 1996, GEOLOGIC MAP OF THE ISLAND OF HAWAII: , p. 20.

Wyatt, M.B., and McSween, H.Y., 2002, Spectral evidence for weathered basalt as an alternative to andesite in the northern lowlands of Mars: Nature, v. 417, p. 263–266, doi:10.1038/417263a.